Critical gravitational collapse of a perfect fluid: Nonspherical perturbations

Carsten Gundlach
Enrico Fermi Institute, University of Chicago, 5640 South Ellis Avenue, Chicago, Illinois 60637
*and Faculty of Mathematical Studies, University of Southampton, Southampton SO17 1BJ, United Kingdom**
(Received 9 October 2001; published 29 March 2002)

Continuously self-similar (CSS) solutions for the gravitational collapse of a spherically symmetric perfect fluid, with the equation of state $p=\kappa\rho$, with $0<\kappa<1$ a constant, are constructed numerically and their linear perturbations, both spherical and nonspherical, are investigated. The $l=1$ axial perturbations admit an analytical treatment. All others are studied numerically. For intermediate equations of state, with $1/9<\kappa\lesssim 0.49$, the CSS solution has one spherical growing mode, but no nonspherical growing modes. That suggests that it is a critical solution even in (slightly) nonspherical collapse. For this range of κ we predict the critical exponent for the black hole angular momentum to be $5(1+3\kappa)/3(1+\kappa)$ times the critical exponent for the black hole mass. For $\kappa=1/3$ this gives an angular momentum critical exponent of $\mu\simeq 0.898$, correcting a previous result. For stiff equations of state, $0.49\lesssim\kappa<1$, the CSS solution has one spherical and several nonspherical growing modes. For soft equations of state, $0<\kappa<1/9$, the CSS solution has $1+3$ growing modes: a spherical one, and an $l=1$ axial mode (with $m=-1,0,1$).

DOI: 10.1103/PhysRevD.65.084021 PACS number(s): 04.40.Nr, 04.25.Dm, 04.70.Bw, 05.70.Jk

I. INTRODUCTION

An isolated system in general relativity ends up in one of three stable final states: a black hole, a star, or complete dispersion. The phase space of isolated systems in general relativity is therefore divided into basins of attraction: each initial data set must end up in one of the stable end states. The study of the boundaries between the basins of attraction, in particular of the boundary between the black hole and dispersion end states, began with the pioneering work of Choptuik [1], and is now an active field in classical general relativity.

Initial data near the black hole or dispersion threshold evolve through a universal intermediate state before dispersing or forming a black hole. This intermediate attractor has higher symmetry, as a spacetime, than the generic solution. Often it is self-similar. Close to the threshold, but on the collapse side, the mass of the final black hole then scales as a universal power of the distance of the initial data to the black hole threshold. Universality, self-similarity and the critical exponent for the black hole mass have given rise to the name (type II) ''critical phenomena in gravitational collapse.'' For a review see [2].

Critical phenomena of this type are explained by the existence of a solution that is self-similar, regular, and has exactly one growing perturbation mode, such that for one sign of the growing mode the solution veers towards black hole formation, and for the other towards collapse. Such a solution is called a (type II) critical solution. From a dynamical systems point of view, a critical solution is an attractor within the black hole threshold, which is a hypersurface of codimension one. Within the complete phase space, it is therefore an attractor of codimension one. All solutions that start near the black hole threshold, but not necessarily near the critical solution itself, are funneled through this intermediate attractor. This funneling process explains both universality and the self-similar nature of the intermediate attractor explains scaling. The critical exponent in the power-law scaling of the black hole mass can be shown to be the inverse of the Lyapunov exponent of the critical solution's one growing perturbation mode [3].

Here we concentrate on one class of matter models coupled to general relativity, perfect fluids with the linear baryotropic equation of state $p=\kappa\rho$, where p is the pressure, ρ is the total energy density measured in the rest frame, and κ is a constant in the range $0<\kappa<1$. The spherically symmetric fluid with $\kappa=1/3$, corresponding to an ultrarelativistic gas, was one of the first systems in which critical phenomena were found [4]. These results were later extended to the range $0<\kappa<1$ [5–7]. We now ask what happens when we allow small deviations from spherical symmetry.

For a sample of values of κ in the range $0<\kappa<1$, we construct a regular, continuously self-similar (CSS), and spherically symmetric solution, and then investigate its linear perturbations to see how many growing perturbation modes it has. It is already known, from both perturbative [5,6] and non-perturbative [7] calculations that these solutions have exactly one growing mode among their spherically symmetric perturbations, which makes them critical solutions in spherical symmetry. Here we examine their nonspherical perturbations. In a previous Rapid Communication [8] we examined the particular case $\kappa=1/3$. Here we generalize this investigation to all values of κ in the range $0<\kappa<1$. We also describe our numerical methods and results in much more detail. Finally, we correct two incorrect assumptions in [8], namely that the $l=1$ axial perturbations obey the same type of equation as the $l\geqslant 2$ ones, and that the $l=1$ polar perturbations are pure gauge. As it happens, correcting these errors does not affect the overall conclusion of Ref. [8], namely that the critical solution for $\kappa=1/3$ has no growing nonspherical perturbation modes.

As the background is spherically symmetric, the perturbations can be separated into spherical harmonics labeled by l

*Current address.

and m, and can be split further into axial and polar parts. The perturbation equations we use are those derived in [9], restricted here to a CSS background and the particular equation of state $p=\kappa\rho$. Surprisingly, the nonspherical perturbation equations are much harder to solve numerically than in the equivalent problem for the massless scalar field [10]. One difficulty is that we are dealing with a one-parameter family of background solutions, whose limits $\kappa=0$ and $\kappa=1$ are not regular members of the family. The other difficulty is that in the $l\geqslant 2$ perturbations both light cones and sound cones play a dynamical role, while they coincide for the scalar field. This gives rise to weak solutions (in the sense of hyperbolic equations) that we need to discard. Because of these problems, our final choice of numerical approach is to discretize the perturbation evolution equations in space but not in time. We then look directly for eigenvectors and eigenvalues (modes) of the finite difference equations.

The plan of the paper is this: in Sec. II we discuss the general perturbation framework of Ref. [9], and the CSS background solutions. Section III discusses the $l=1$ axial perturbations. Their spectrum can be calculated in closed form. Based on this, we correct the value of the angular momentum critical exponent stated in Ref. [11]. All other perturbations require a numerical treatment and are discussed in Sec. IV. Details of the numerical difficulties and numerical methods, however, are given in the Appendixes. Section V summarizes our results.

II. BACKGROUND SOLUTION

A. Perturbations of a spherically symmetric perfect fluid

We shall examine the linear perturbations of a spherically symmetric and continuously self-similar (CSS) perfect fluid spacetime. For this purpose we use the restriction to a CSS background of a general framework for the perturbations of time-dependent spherically symmetric perfect fluid solutions that was presented in [9]. In this formalism, the spacetime manifold is written as the product $M=M^2\times S^2$, where S^2 is the 2-sphere and M^2 is a 2-dimensional manifold, the "rt-plane," with a boundary $r=0$. The coordinates in M^2 are denoted by x^A, and the coordinates in S^2 by x^a. Coordinates in all of M are collectively denoted by x^μ. The general spherically symmetric metric becomes, in this notation,

$$g_{\mu\nu}\equiv \mathrm{diag}(g_{AB},r^2\gamma_{ab}), \tag{1}$$

where r^2 is a scalar function on M^2, and γ_{ab} is the unit metric on S^2. The spherically symmetric perfect fluid stress-energy tensor can be written in the same notation as

$$T_{\mu\nu}\equiv \mathrm{diag}(\rho\, u_A u_B+p\, n_A n_B, p\, r^2\gamma_{ab}), \tag{2}$$

where ρ and p are the (total) energy density and pressure in the fluid rest frame, $u^\mu=(u^A,0)$ is the fluid 4-velocity, and n^A is the outward pointing unit vector normal to u^A in M^2. The field equations in this framework are covariant in M^2. The two extra dimensions in S^2 appear through the scalar r.

The perturbations of a spherically symmetric background decompose naturally into polar and axial parity, and into spherical harmonic angular dependencies, for different l and m. The equations of motions are the same for all values of $-l\leqslant m\leqslant l$, for given $l\geqslant 0$. The cases $l=0$, $l=1$ (polar and axial), and $l\geqslant 2$ (polar and axial) are all qualitatively different and need to be treated separately. Tensors in M, including the perturbations, are written as products of tensors in M^2 with tensors in S^2. All necessary tensors in S^2 are built from the scalar spherical harmonics Y_{lm} on S^2, their covariant (with respect to γ_{ab}) derivatives, and the covariantly constant antisymmetric tensor ϵ_{ab}. The final equations for the perturbations are again covariant equations for tensors on M^2. Their angular dependence comes in through terms such as l/r and $l(l+1)/r^2$.

In the next step, linear combinations of the perturbations are found that do not change to linear order under infinitesimal coordinate transformations, in either M^2 or S^2. The perturbation equations can be rewritten in terms of these gauge-invariant perturbations alone.

In a further step, all perturbation tensors in M^2 are split into frame components with respect to the orthonormal frame (u^A,n^A). This "scalarization" replaces covariant derivatives of tensors with partial derivatives of scalars. These derivatives are also decomposed into their frame components $\dot f\equiv u^A f_{,A}$ and $f'\equiv n^A f_{,A}$. The perturbation equations are now scalar equations written without reference to a particular coordinate system. In this sense they are covariant, as well as linearly gauge-invariant. Note that the frame derivatives are not partial derivatives, and do not commute. The advantage of using these derivatives is that $\dot f\pm c_s f'$ are derivatives along radial matter characteristics, and $\dot f\pm f'$ derivatives along the radial light rays. On the other hand, some constraint-type perturbation equations for $l=0$ and $l=1$ are most naturally written using the derivative $D\equiv r\partial f/\partial r$ along polar slices.

In a final step, we rescale the perturbation variables by l-dependent powers of r so that they are either $O(1)$ at the origin and even functions of r, or else $O(r)$ and odd. The equations are brought into first-order form by treating first derivatives such as $\dot f$ and f' as independent variables where necessary.

In the remainder of this section, we introduce coordinates that are adapted to a CSS background, and review how the background solution is defined, and constructed numerically.

B. Continuously self-similar background solution

Although our perturbation variables are linearly gauge-invariant, we have to choose a coordinate system on the background. A standard choice of coordinates x^A is to use r as a coordinate (radial gauge), and make the second coordinate t orthogonal to it (polar slicing). Then g_{AB} takes the form

$$g_{tt}=-\alpha^2,\quad g_{rr}=a^2,\quad g_{rt}=0, \tag{3}$$

with α and a functions of r and t. Radial light rays are governed by the combination $g\equiv a/\alpha$. There is a remaining gauge freedom $t\to t'(t)$, and we fix it by setting $\alpha=1$ at $r=0$ for all t.

Based on radial-polar coordinates, we now introduce coordinates that are adapted to self-similarity, while retaining polar slicing. We define new coordinates x and τ by

$$r \equiv sxe^{-\tau}, \quad t \equiv -e^{-\tau}, \tag{4}$$

with $s>0$ a constant. We have assumed that $t<0$, and have chosen signs so that τ increases as t increases. Note that $\tau \to \infty$ as $t \to 0_-$. Partial derivatives transform as

$$f_{,t} = e^{\tau}(f_{,\tau} + x f_{,x}), \quad f_{,r} = s^{-1} e^{\tau} f_{,x}. \tag{5}$$

The metric g_{AB} in these coordinates becomes

$$g_{\tau\tau} = e^{-2\tau}(-\alpha^2 + s^2 x^2 a^2), \quad g_{xx} = e^{-2\tau} s^2 a^2,$$
$$g_{\tau x} = -e^{-2\tau} s^2 x a^2. \tag{6}$$

The spacetime is continuously self-similar (with homothetic vector $-\partial/\partial\tau$) if and only if α and a depend only on x but not on τ. τ has two different interpretations. On the one hand, it is a time coordinate in the sense that its level surfaces are spacelike. But $-\tau$ is also the logarithm of spacetime scale, in the sense that proper distances are proportional to intervals Δx and $\Delta\tau$ times a factor of $e^{-\tau}$. In a self-similar spacetime, larger τ therefore means structure on a smaller scale. The point $r=0$, $t=0$, or $\tau=\infty$, is by construction a curvature singularity, unless the spacetime is flat.

In the solutions we consider here the matter is a perfect fluid with density ρ and pressure $p=\kappa\rho$, with κ a constant. This equation of state is the only one compatible with exact self-similarity. We impose CSS in the metric by making the ansatz $a=a(x)$ and $\alpha=\alpha(x)$. Imposing self-similarity on the spacetime, we find from the Einstein equations that $4\pi\rho = e^{2\tau}\overline{\rho}(x)$ and $V \equiv u^A r_{,A}/n^B r_{,B} = V(x)$. Here $n^A \equiv -\epsilon^A{}_B u^B$ is the outward-pointing unit spacelike vector normal to u^A. The constant s that was introduced above is now chosen so that the surface $x=1$ is a matter characteristic. It is then the past sound cone of the singularity.

The background solution that we want to use is completely defined by the assumptions of (i) continuous self-similarity, (ii) spherical symmetry, (iii) analyticity at the center $x=0$, and (iv) analyticity at the past sound cone $x=1$. The background equations resulting from the CSS ansatz are given in Appendix A. The CSS ansatz reduces the two Einstein equations and two matter equations that are needed in spherical symmetry to one algebraic equation for a and three ordinary differential equations in x for ρ, V and $g \equiv a/\alpha$.

There are two boundary conditions for a CSS solution at $x=0$. The gauge condition $\alpha(0)=1$ becomes $g(0)=1$. From regularity of the matter velocity, CSS, and matter conservation one can derive that

$$\lim_{x\to 0} \frac{V}{sgx} = -\frac{2}{3(1+\kappa)}. \tag{7}$$

Imposing this is the regularity condition (iii) at the center. Note that this limit would also hold for a CSS fluid in a flat spacetime.

One boundary condition at $x=1$ is the gauge condition $D(1)=0$, which makes $x=1$ the sound cone. This condition determines the value of the constant s. The regularity condition (iv) at the sound cone is

$$\sqrt{\kappa} S_1(1) = S_2(1), \tag{8}$$

which is the vanishing of the term in the equations that is divided by D (see Appendix A).

Once we have solved the boundary value problem in $0 \leqslant x \leqslant 1$, we can analytically continue the solution through $x=1$ (which is a regular singular point of the equations) and then continue the solution by evolving the ODEs to larger x. (In numerical terms, analytic continuation is implemented by polynomial extrapolation.) We go to the light cone and a little beyond. The light cone is at a value of x that depends on κ. The ODEs are regular there.

Our numerical method for imposing analyticity at $x=1$ and $x=0$ is to just impose the algebraic boundary conditions there, and to use centered differences everywhere else, without using an explicit power-law expansion about the singular points. The first (numerical) derivative of the fluid density and velocity profiles obtained with this method has a small discontinuity at $x=1$ that first appears at $\kappa \simeq 0.7$ and increases with κ. Results for $\kappa \gtrsim 0.7$ therefore have a source of numerical error over and above the one arising in the numerical evolution of the perturbations.

III. AXIAL $l=1$ PERTURBATIONS—ANALYTICAL TREATMENT

A. Equation of motion

In this section we discuss the axial $l=1$ perturbations of the continuously self-similar perfect fluid critical solution. This leads us, from general arguments given in [11], to a prediction for the scaling of black hole angular momentum in critical collapse. Note that this section differs from the rest of the paper in presenting purely analytical results.

The axial $l=1$ perturbations contain a single matter degree of freedom, and no gravitational waves. The gauge-invariant fluid velocity perturbation, β, obeys the autonomous equation of motion

$$(\beta r^2 \rho u^A)_{|A} = 0. \tag{9}$$

This is just a transport equation along the background fluid flow. All axial metric perturbations are encoded in a gauge-invariant scalar Π. For $l=1$, Π is obtained from β by quadrature, and Eq. (9) describes the dynamics completely. For $l \geqslant 2$, Π obeys a wave equation with a source term proportional to β. (In [11], it was incorrectly assumed that this is true also for $l=1$.)

As we shall see now, the complete mode spectrum of β can be obtained analytically for all l. For $l=1$, we then have the complete dynamics. For $l \geqslant 2$, the spectrum of β is also known analytically, but that of the homogeneous Π modes must be calculated numerically. Here we obtain the modes of β for general $l \geqslant 1$, and restrict to $l=1$ at the end.

The perturbed fluid velocity is regular at $r=0$ if β is $O(r^{l+1})$ there. We therefore define a rescaled variable $\overline{\beta}=r^{-(l+1)}\beta$ that is even in x and generically nonzero at $x=0$. The perturbed stress-energy tensor remains self-similar if β depends on τ as $e^{-\tau}$ at constant x (for any l). We therefore define a rescaled variable $\mathring{\beta}=e^{-l\tau}\overline{\beta}=e^{\tau}(sx)^{-(l+1)}\beta$. This final variable obeys the equation

$$\mathring{\beta}_{,\tau}+\left(x+\frac{V}{sg}\right)\mathring{\beta}_{,x}+\left\{-1+\frac{\kappa}{1+\kappa}\left[2+\left(x+\frac{V}{sg}\right)(\ln\overline{\rho})_{,x}\right]+(l+1)\left(1+\frac{V}{gsx}\right)\right\}\mathring{\beta}=0. \tag{10}$$

This is of the form

$$\mathring{\beta}_{,\tau}+xA(x)\mathring{\beta}_{,x}+B(x)\mathring{\beta}=0, \tag{11}$$

where A and B are regular, even, strictly positive functions of x, so that $A(x)=A_0+A_2x^2+O(x^4)$, and similarly $B(x)=B_0+B_2x^2+O(x^4)$. We look for solutions $\mathring{\beta}$ that are regular even functions of x.

B. Analytic calculation of the mode spectrum

Using the method of characteristics, the general solution of Eq. (11) can be written as

$$\mathring{\beta}(x,\tau)=e^{-B_0\tau}\exp\left(-\int_0^x\frac{B(x)-B_0}{xA(x)}dx\right)\times F\left[x\exp\left(-\int_0^x\frac{A(x)-A_0}{xA(x)}dx-A_0\tau\right)\right], \tag{12}$$

where $F(z)$ is a free function that is determined by the initial data. Note that the two definite integrals exist and are $O(x^2)$. For regular, even initial data, with $\mathring{\beta}(x,0)=F_0+O(x^2)$, we have $F(z)=F_0+O(z^2)$.

We can now read off that the late-time behavior of the solution $\mathring{\beta}(x,\tau)$ as $\tau\to\infty$ is

$$\mathring{\beta}(x,\tau)=e^{-B_0\tau}[F_0+O(x^2)+O(e^{-2A_0\tau})] \tag{13}$$

as $\tau\to\infty$. For generic regular initial data, F_0 does not vanish, and the solution decays as $e^{-B_0\tau}$ at late times. One might have expected that the growth exponent depends on details of the background, but in fact it depends only on the background at the center. The physical reason for this is that the transport equation transmits information only from the center outwards. For example, we can see from Eq. (12) that the solution $\mathring{\beta}$ for initial data that vanish in a neighborhood of $x=0$ is strictly zero at any fixed x at sufficiently large τ.

Surprisingly again, we can evaluate B_0 in closed form, even though the background solution away from the center is known only numerically. From matter conservation and the assumption of continuous self-similarity we have the regularity condition (7). When we also take into account that $\overline{\rho}$ is an even function of x and that v is an odd function, we find from Eq. (10) that

$$\lambda=-B_0=\frac{2(1-3\kappa)-(1+3\kappa)l}{3(1+\kappa)}. \tag{14}$$

This analytic result is in perfect agreement with the late time behavior of numerical evolutions of generic initial data for $\mathring{\beta}$.

We now show that the mode spectrum is discrete. To look for modes, we make the ansatz

$$\mathring{\beta}(x,\tau)=e^{\lambda\tau}f(x) \tag{15}$$

and obtain

$$x\frac{df}{dx}=-\frac{\lambda+B}{A}f. \tag{16}$$

By expanding this equation in powers of x around $x=0$ and comparing coefficients, we see that if $f(0)\neq 0$, and f is to be a regular even function of x, we must have $\lambda=-B_0$. This is precisely the mode that dominates the late-time behavior (13), and we may call it $f_0(x)$. One obtains it as a power series in a neighborhood of $x=0$, and then by solution of the ODE (16). We normalize f_0 by setting $f_0(0)=1$. We now subtract a suitable multiple of this mode from the solution $\mathring{\beta}$ to obtain something that is $O(x^2)$ at $x=0$:

$$\mathring{\beta}^{(2)}(x,\tau)\equiv\mathring{\beta}(x,\tau)-F_0e^{-B_0\tau}f_0(x) \tag{17}$$

where $\mathring{\beta}(x,0)=F_0+O(x^2)$ as before. By construction $\mathring{\beta}^{(2)}(x,0)=O(x^2)$. Expanding Eq. (12) to the next order, we have

$$\mathring{\beta}^{(2)}(x,\tau)=e^{-(B_0+2A_0)\tau}[F_2+O(x^2)+O(e^{-2A_0\tau})]x^2. \tag{18}$$

We then obtain a mode $f_2(x)$ by solving Eq. (16) with $\lambda=-(B_0+2A_0)$. We normalize it as $f_2(x)=x^2+O(x^4)$. Continuing in this way, we can strip off a sequence of modes decaying with $\lambda=-(B_0+2nA_0)$ for $n=0,1,2,\ldots$. These modes are $O(x^{2n})$ at the origin, and so form a complete basis for smooth functions $\mathring{\beta}$. Therefore the entire spectrum is discrete.

From Eq. (10), using again Eq. (7), we find

$$A_0=\frac{1+3\kappa}{3(1+\kappa)}. \tag{19}$$

We can now write down the complete spectrum for all values of κ and l, labeled by the index $n=0,1,2,\ldots$. It is

$$\lambda(\kappa,l,n)=-B_0(\kappa,l)-2nA_0(\kappa)=\frac{2(1-3\kappa)-(1+3\kappa)(l+2n)}{3(1+\kappa)}. \tag{20}$$

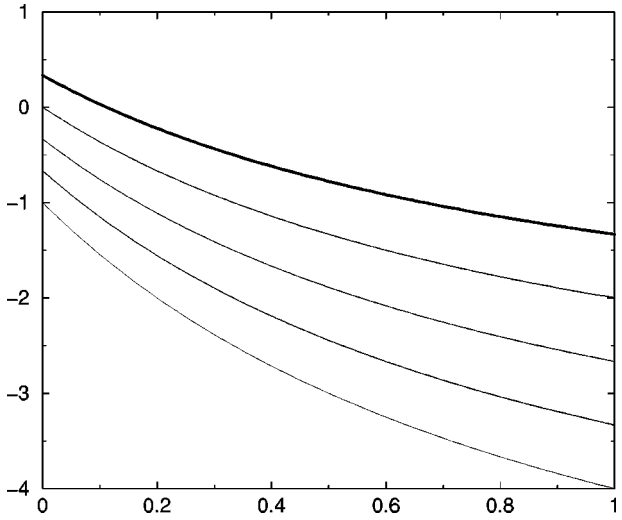

FIG. 1. The $\mathring{\beta}$ equation describes axial fluid velocity perturbations. The plot shows the growth exponent λ, which is real, against κ. We plot $\lambda(\kappa,l,n)$ given in Eq. (20). The thick line is for $l=1$ and $n=0$, where $\mathring{\beta}$ is the only perturbation. (It is positive for $\kappa<1/9$.) Below, from top to bottom $l=2\ldots5$, for the leading mode, with $n=0$.

From this formula we can read off that all $l\geqslant 2$ modes decay for all κ in the range $0<\kappa<1$. All $l=1$ modes also decay for $\kappa>1/9$, but for $\kappa<1/9$ there is exactly one growing $l=1$ mode (the $n=0$ mode). λ for the dominant $(n=0)$ $l=1$ mode is relevant for angular momentum scaling. It is

$$\lambda_1=\frac{1-9\kappa}{3(1+\kappa)}. \tag{21}$$

The dominant $(n=0)$ mode is plotted for $l=1\ldots5$ in Fig. 1.

C. Angular momentum scaling

In [11] we derived a general formula for the critical exponent μ governing black hole angular momentum in critical collapse, namely

$$\mu=\frac{2-\lambda_1}{\lambda_0}=(2-\lambda_1)\gamma. \tag{22}$$

[This formula corrects a misprint in Eq. (11) of Ref. [11].] Here λ_0 is the Lyapunov exponent for the spherical mode, which is real and positive, and $\lambda_1\equiv\lambda(\kappa,1,0)$ is the Lyapunov exponent for the $l=1$ axial perturbations, which are real. $\gamma=1/\lambda_0$ is the critical exponent for the black hole mass. The derivation of this formula assumes that the critical solution has precisely one growing perturbation mode, which is spherically symmetric, while all nonspherical perturbation modes decay. The analytical result in this section and the numerical results in the following sections show that this assumption holds in the range $1/9<\kappa\lesssim 0.49$.

For this range of equations of state, putting the results (21) and (22) together, we obtain the analytical prediction

$$\mu(\kappa)=\frac{5(1+3\kappa)}{3(1+\kappa)}\gamma(\kappa),\quad \frac{1}{9}<\kappa\lesssim 0.49, \tag{23}$$

for the angular momentum exponent μ, given the mass exponent γ.

This result corrects the value of μ given in [11] for the case $\kappa=1/3$, based on an incorrect value of λ_1. The correct value $\lambda_1=-1/2$ for $\kappa=1/3$ gives a real critical exponent $\mu=5\gamma/2\simeq 0.898$ for the black hole angular momentum. Note that the incorrect value given in [11] was complex, which was expected to give rise to oscillations in the direction of the black hole angular momentum as the black hole threshold is approached. However, the correct value of λ_1 is real, and so the angular momentum scaling is a power law, like the mass scaling.

IV. ALL OTHER PERTURBATIONS—NUMERICAL TREATMENT

A. General aspects of the perturbation equations

Before we discuss the perturbation equations of motion in detail, it is useful to discuss the general form of the perturbations of a spherically symmetric and CSS solution. As we have seen, we can choose dependent and independent variables for the background so that the background is given by a number of functions $Z(x,\tau)=Z_*(x)$ of a single self-similarity variable x. It follows that the equations of motion of the linear perturbations of this background, when written in first-order form in suitable variables, are of the general form

$$u_{,\tau}=A(x)u_{,x}+B(x)u, \tag{24}$$

$$u_{,x}=C(x)u. \tag{25}$$

Here $u(x,\tau)$ is a vector of perturbations, and A, B, C are matrices that depend on the background. We shall call the coupled partial differential equations that contain τ-derivatives evolution equations, and the coupled ordinary differential equations in x constraints. Not all variables u need obey both types of equation—some variables u obey only an evolution equation, others only a constraint equation, and yet others both. For most of the perturbations, we shall be able to use a free evolution scheme in which the only constraints are trivial ones of the form $u_{1,x}=u_2$ introduced by writing a wave equation in first-order form. For the spherical perturbations and the polar $l=1$ perturbations, however, it is unavoidable to solve nontrivial constraint equations.

The perturbation equations (24),(25) admit solutions of the form

$$u(x,\tau)=e^{\lambda\tau}u_\lambda(x). \tag{26}$$

Both λ and $u_\lambda(x)$ are in general complex, but because the coefficients A, B and C are real, the solutions form complex conjugate pairs. With $\lambda\equiv\Lambda\pm i\omega$, the general real solution is

$$\mathrm{Re}[Ce^{i\delta}u(x,\tau)] = Ce^{\Lambda\tau}[\cos(\omega\tau+\delta)\mathrm{Re}\,u_\lambda(x) - \sin(\omega\tau+\delta)\mathrm{Im}\,u_\lambda(x)]. \quad (27)$$

If the general solution can be written as a sum over such modes is a subtle question, but here we ask mainly if there are any growing modes with $\Lambda>0$. Furthermore, if we discretize $u(x,\tau)$ on a finite grid in x (but not in τ), the general solution of the discretized field equations is then clearly given by the sum over a finite number of modes, each of which is exactly exponential in τ.

In defining the variables u that we evolve numerically, we begin from all the variables with an overbar defined in [9], and their dot and dash derivatives where necessary. On a self-similar background, it is useful to further rescale these variables by powers of e^τ so that the background plus perturbations is still self-similar if and only if the rescaled variables are independent of τ. If this is done, the resulting equations do not contain explicit powers of e^τ. The spacetime perturbations grow in a physical sense towards the singularity if and only if the variables u grow with τ. Rescaled barred variables will be denoted by a circle, their rescaled dot derivatives by a tilde, and their rescaled prime derivatives by a hat.

In the following, we shall use ''degree of freedom'' to denote a variable that can be freely specified as a function of a radius at the initial moment of time. In this count, a wave equation has two degrees of freedom, for each value l and m. In the $l\geqslant 2$ perturbations there are eight physical degrees of freedom, corresponding to wave equations for the two polarizations of gravitational waves, the three components of the Euler equation, and the continuity equation. On a spherically symmetric background, these generic eight degrees of freedom split into three axial and five polar degrees of freedom. The number of first-order variables is larger (four and seven, respectively) because in the first-order form of a wave equation for a variable ϕ, ϕ itself and $\phi_{,x}$ are separate variables that are linked by a (trivial) constraint equation.

B. Numerical methods

In investigating the non-spherical perturbations numerically, we have to treat each value of κ and l separately. (The equations do not depend on m.) In practice, we work with a finite sample of values of κ in the range $0<\kappa<1$, and with $l\leqslant 5$. With increasing l, numerical difficulties at the center of spherical symmetry become more pronounced, limiting the range of l we can investigate. Fortunately the range $l\leqslant 5$ is sufficient to see a trend, as we shall demonstrate in plots.

We are looking for mode solutions of the form (26), and in particular for the dominant mode, the one with the lowest value of $\Lambda\equiv\mathrm{Re}\,\lambda$. This objective allows a number of very different numerical approaches. Three different ones come to mind, and we describe them first, and then summarize our experience with the last two of them. More details are given in the Appendixes.

(1) Making the ansatz (26), and imposing suitable regularity conditions, one obtains a boundary value problem for an eigenvector $u_\lambda(x)$ and eigenvalue λ. For the $l\geqslant 2$ axial perturbations, regularity conditions have to be imposed at the center and at the light cone. For the $l=1$ polar perturbations regularity conditions have to be imposed at the center and the soundcone, and for the $l\geqslant 2$ polar perturbations regularity conditions are required at the center and both the light cone and the soundcone (which is in the interior of the numerical domain). Modes can then be found in two ways:

(a) From an initial guess for λ and $u_\lambda(x)$, one can find the correct values by shooting or relaxation. In practice, the initial guess has to be quite good, and finding one solution does not exclude the possibility that there is another solution with larger Λ.

(b) For given λ, the boundary (and possibly midpoint) conditions can be solved in terms of n free parameters. If the boundary value problem is well-posed, the shooting procedure must match up n variables. The mismatch in these n variables is a linear function of the n free parameters, and is therefore described by an $n\times n$ matrix A that depends analytically on λ. If $A(\lambda)$ has a kernel, a solution u_λ can be found for this λ. One therefore looks for zeros of the complex-analytic function $\det A(\lambda)$. This can be done by contour integrals [12].

(2) One can also use the equations to evolve generic initial data $u(x)$ in τ. At late times the solution will be dominated by the dominant mode, and one can read off λ from its time dependence. One can also subtract the dominant modes one after another, in the Gram-Schmidt process, in order to find subdominant modes. This is known as the Lyapunov method [6].

(3) In a third approach, the evolution equations are finite differenced in x but not in τ. The resulting finite difference-differential equations can be used in two ways:

(a) With M degrees of freedom on N grid points in x, the map $T:u_i(x_j)\to u_{i,\tau}(x_j)$ with $i=1\ldots M$ and $j=1\ldots N$ is a square matrix of size $(MN)^2$. Its eigenvalues with the largest real parts should be an approximation to the continuum eigenvalues λ with largest real part. (The lower eigenvalues will depend on the discretization scheme and are not expected to correspond to continuum modes.)

(b) Alternatively, we can use a standard ordinary differential equation (ODE) integration scheme to discretize in time. Such a numerical method is called ''semi-discrete'' because with sufficiently small step size $\Delta\tau$ it is effectively discrete only in x. The map $T_\Delta:u(0,x)\to u(\Delta,x)$ for a finite interval Δ is again an $(MN)^2$ matrix. The few eigenvalues with largest modulus should now be approximations to the largest of the numbers $e^{\Delta\tau}$.

We first implemented the Lyapunov, method (2). It is the simplest method for obtaining the dominant mode. This method worked well for the $\kappa=1/3$ fluid [8], and also for the nonspherical perturbations of the scalar field critical solution [10]. However, in the polar perturbations for some values of κ and l, the dominant mode is a numerical artifact (an instability) in all finite differencing schemes that we have tried. (The nature of the instabilities will be discussed below.) Then one needs to look for sub-dominant modes of the finite difference equations in order to find the dominant physical mode. We have found that the Lyapunov method is extremely inefficient for finding subdominant modes.

We then implemented both methods (3a) and (3b). In method (3b) we used first order, second order and fourth order Runge-Kutta integration (RK1, RK2, RK4), and an implicit second-order scheme (iterated Crank-Nicholson, or ICN). For small enough time steps, the differences between these methods are negligible, and we effectively reach the continuum limit in τ. Furthermore, in this limit, the modes and eigenvalues produced by methods (3a) and (3b) agree up to roundoff error. Therefore, there is no advantage in method (3b) over (3a), but a higher computational cost.

Within method (3), many ways of finite differencing in x are possible. We have used four finite differencing schemes in x. The differences between them remain important at all feasible values of Δx. Two of these schemes are upwind schemes that explicitly use the eigenvalues of the matrix A. Both are the linearized version of Godunov schemes. GD1, the scheme used before in [8], is first-order accurate. GD2 is a second-order accurate version. The other two schemes used centered differences and are second-order accurate. CD3 uses the obvious centered differences. CD4 uses a well-known trick to deal with terms of the form $\phi_{,x}+(2l/x)\phi$, which can give rise to numerical instabilities near the center $x=0$. (The 3 and 4 are just consecutive labels.) All four schemes are defined in Appendix E.

Some of the numerical instabilities that we see are familiar: problems at the center, in particular for high l, and grid modes in centered differencing. Another kind of instability was harder to understand. The continuum equations admit mode solutions (26) in which $u_{,x}$ is discontinuous at a characteristic that is also a line of constant x, that is, at the light cone and/or the sound cone of the singularity. The evolution equations are hyperbolic, and these solutions are called weak solutions. They are discussed in more detail in Appendix F. While they are valid as a generalized type of solution, these modes would not arise in a collapse situation, and so we need to exclude them. Unfortunately, for certain values of κ and l, they dominate the top smooth physical mode.

The weak modes were not seen in the investigation [10] of the perturbations of the scalar field critical solution, because there they could be discontinuous only at the light cone of the singularity, but the numerical domain was truncated precisely there. The same can be done for the axial perturbations of the perfect fluid critical solution, because there are no axial sound waves. Similarly, the numerical domain can be truncated at the sound cone for the spherical and $l=1$ polar perturbations because they do not comprise gravitational waves. The $l\geqslant 2$ polar perturbations, however, contain coupled sound and gravitational waves. Therefore the numerical domain cannot be truncated at smaller x than at the light cone, and this leaves weak modes at the sound cone.

The finite differencing schemes we use are not designed to represent weak solutions correctly, but they do of course have a counterpart in the modes of the finite difference system. Sometimes the numerical counterpart resembles the continuum mode (in particular in GD1 and GD2), but sometimes it cannot be distinguished by inspection from a smooth mode (in particular in CD3 and CD4). The only certain criterium is convergence. This makes it crucial that we have more than one finite differencing scheme, so that we can carry out independent residual evaluations, as well as simple convergence tests.

We have loosely referred to the numerical artifacts as instabilities. However, the usual concept of the stability of a numerical method is at most exponential growth of numerical solutions. But here we are using semi-discrete methods (discrete only in x) on a system of linear equations with τ-independent coefficients. Therefore all solutions, both physical and artificial, depend exactly exponentially on τ. Exponential growth, or its absence, can therefore not be used to distinguish between physical and unphysical solutions. An unphysical mode may grow either more or less rapidly than a physical mode. The only certain way of distinguishing them is by convergence. (This will also rule out the weak modes, because the numerical methods were not designed to handle them, and will therefore fail to converge on them.)

We have carried out two kinds of convergence tests. One test is to check that the discretized eigenvectors $u_\lambda(x_j)$ and corresponding eigenvalues λ converge with increasing resolution in x at the expected rate (to first order or second order) for each scheme, but also that all four schemes converge to the same solution. The other test is independent residual evaluation. Writing the system of continuum equations formally as $u_{,\tau}(x)=Lu(x)$, where L is a linear derivative operator, let L_1 and L_2 be two different finite difference approximations to L, and let (u_1,λ_1) and (u_2,λ_2) be modes (eigenvectors and eigenvalues) of L_1 and L_2. If these are approximations to a continuum mode, the norms $|\lambda_1 u_1 - L_2 u_1|$ and $|\lambda_2 u_2 - L_1 u_2|$ should converge to zero with increasing resolution. Convergence should be to second order in resolution if both methods are second-order accurate, and to first order in resolution if one or both methods are only first-order accurate. For the norm $||$ we choose the l_2 norm divided by the number N of grid points, which is an approximation to the L_2 norm.

Imposing the constraints (25) poses no numerical difficulty. During evolution, in methods (2) or (3b), one has the choice of either imposing the constraints only on the initial data, from time to time, or at each time step. We find that this hardly affects the results. Some care has to be taken when calculating the map T in the presence of constraints. This is discussed in Appendix G.

C. Spherical perturbations

The spherical perturbations have already been investigated by several authors [5–7], and we use them here as a test of our methods, and also to make sure that we are investigating the same background solution as these authors. Gauge-invariant perturbations do not exist for $l=0$. Equations of motion for the spherical perturbations are most easily obtained by linearizing the field equations in spherical symmetry in the polar-radial gauge that is also used for the background. The perturbations $\delta(\ln\rho)$ and δV obey evolution equations in τ and x, while the perturbations δa and δg obey constraint equations in x only. We do not give the detailed equations here.

We have used all four codes. In GD1, GD2 and CD3 the top physical (growing) mode shows up as the top numerical

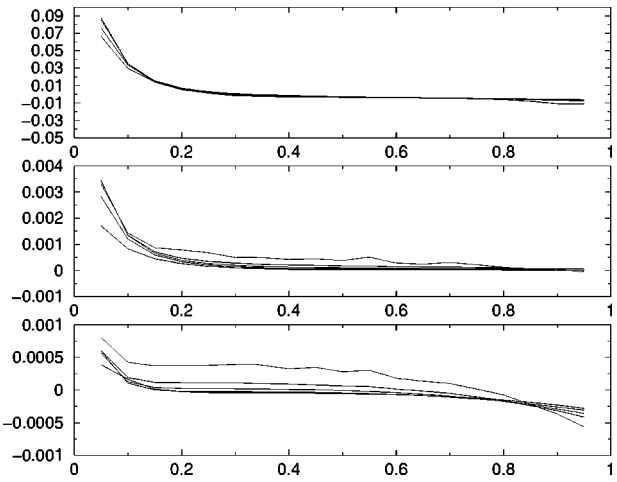

FIG. 2. This plot demonstrates that $\lambda(\kappa)$ in GD1, GD2 and CD3 converges with increasing resolution to a common value and at the expected order. The resolutions are $\Delta x = 1/10, 1/20, \ldots 1/320$. The three plots, from top to bottom, show the error in GD1, GD2 and CD3. A reference value for $\lambda(k)$ was obtained by Richardson interpolation on CD3 at the highest three resolutions. This reference value was then subtracted from the result of all three codes at all resolutions to obtain a measure of error. To demonstrate power-law convergence, this error was divided by a factor of 4 for each factor of 2 in Δx (for CD3 and GD2), or by a factor of 2 (for GD1). The error at the highest resolution was not rescaled. Note the rise of the error at low κ in all three methods. Although the different graphs in each plot do not lie on top of each other perfectly, they are similar, indicating approximate power-law scaling at the expected order.

mode. In CD4 the growing physical mode is also present but must be identified by hand because it is dominated by grid modes.

Figure 2 demonstrates the convergence of GD1, GD2 and CD3 with increasing resolution towards a common value of $\lambda(k)$ over the entire range of κ. GD1 converges approximately to first order, and GD2 and CD3 approximately to second order, as expected. The finite differencing error is approximately 10^{-3} in both second-order schemes at $\Delta x = 1/320$ for intermediate values of κ. It rises towards the high and the low end of the κ range.

Figures 3 and 4 compare our $\lambda(k)$ at $\Delta x = 1/320$ (GD1, GD2 and CD3) with that obtained by Maison [5]. The results agree quite well for all κ. Nevertheless, the figures show that there is a systematic difference to Maison's results that is generally much larger than our finite difference error. It grows in all three codes as $\kappa \to 1$. (The exception is in GD1 at low κ where the finite difference error becomes dominant.) We suspect that the systematic error is in our code, rather than Maison's code, and specifically in the background code: as we have discussed above, it is not well behaved at the light cone as $\kappa \to 1$, and at the center as $\kappa \to 0$.

D. Axial $l \geqslant 2$ perturbations

For $l \geqslant 2$ the gauge-invariant velocity perturbation β obeys an autonomous transport equation, just as for $l = 1$. For $l \geqslant 2$, there is also a gauge-invariant metric perturbation Π, which obeys a wave equation with β as a source [9]. The

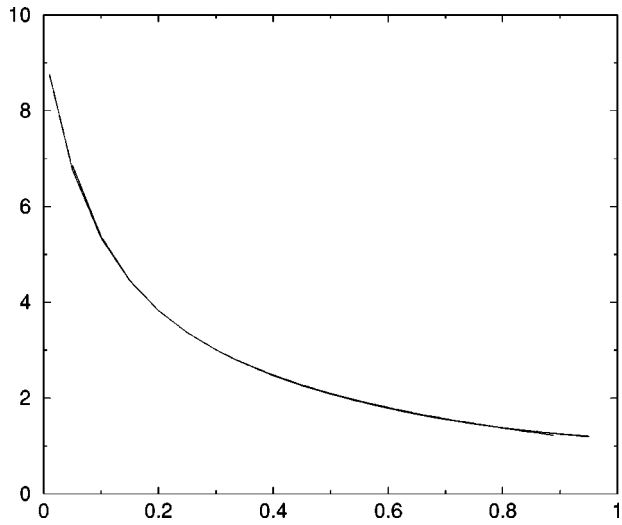

FIG. 3. $\lambda(\kappa)$ from Maison, and our codes GD1, GD2 and CD3 at $\Delta x = 1/320$. (The four lines are not resolved in this plot.)

evolution of β is still autonomous. This means that the λ spectrum of the coupled Π and β system is the sum of two parts: modes in which β vanishes, so that they are solutions of the Π equation without a source term, and modes that are driven by β, so that their value of λ is set by the evolution of β.

As shown above in Sec. III, the spectrum of of β modes can be calculated analytically for all l including $l \geqslant 2$. As a check we have implemented the β equation on its own, and the numerical results agree with the analytical ones, showing the top two of the analytically calculated modes. That is as much as one can expect, because the n-th mode behaves at the center as x^{2n}, and no finite differencing scheme is designed to represent such behavior correctly. In fact, unphysi-

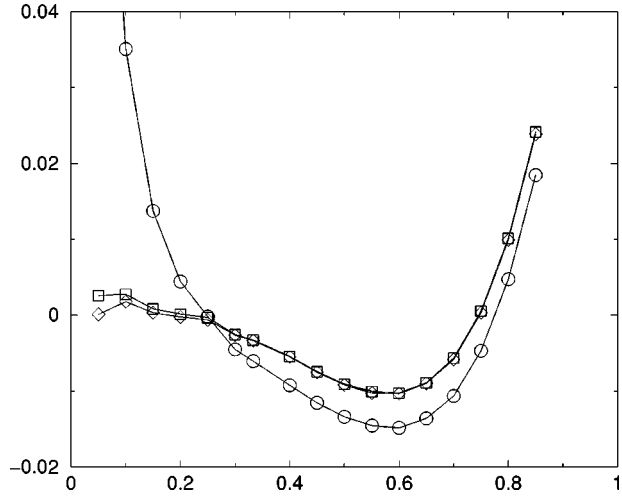

FIG. 4. Difference in $\lambda(k)$ between Maison and our codes at $\Delta x = 1/320$: circles are GD1, squares GD2 and diamonds CD3. The fact that GD2 and CD3 differ from Maison by approximately the same value indicates that this difference is mainly systematic error, rather than finite differencing error. The fact that GD1 has a different deviation from Maison is explained by its larger finite differencing error, which increases at low k—see top plot of Fig. 2.

cal modes that behave as x^n with n odd also show up. They are unphysical because the corresponding velocity perturbation is not regular at the center, but they are valid solutions of the equation.

The equations for Π were derived in the fluid frame in [9], but they look simpler in the frame of constant r observers (radial frame). These are just different choices of first-order variables for the same wave equation. As a test, we have implemented the equations in both frames, and the results converge as expected. In the fluid frame we have also implemented the coupling to β. As expected this simply adds extra modes driven by β modes to the spectrum. As we have analytical results for the β modes (they all decay), we only need the free Π modes.

For simplicity, we give here only the source-free equations in the fluid frame. These equations are quite similar to the toy model wave equation of Appendix D. The variables are

$$\mathring{\Pi} \equiv e^{-l\tau}\overline{\Pi}, \qquad \tilde{\Pi} \equiv e^{-(l+1)\tau}\alpha^{-1}\Pi_{,t},$$
$$\hat{\Pi} \equiv e^{-(l+1)\tau}a^{-1}\Pi_{,r}. \tag{28}$$

$\mathring{\Pi}$ and $\tilde{\Pi}$ can be specified freely on the initial surface, while $\hat{\Pi}$ is constrained by

$$\hat{\Pi} = as\mathring{\Pi}_{,x}. \tag{29}$$

The Π equation without source, in the radial frame, is then equivalent to

$$\tilde{\Pi}_{,\tau} = A_1\tilde{\Pi}_{,x} + B_1\hat{\Pi}_{,x} - \left(l+1+\frac{C_a}{sg}\right)\tilde{\Pi} + \frac{1}{sg}\left[\frac{2(l+1)}{x} + C_\alpha\right]\hat{\Pi} - (l+2)\frac{1}{s^2ag}\left[\frac{C_g}{x} + (l-1)\frac{a^2-1}{x^2}\right]\mathring{\Pi}, \tag{30}$$

$$\hat{\Pi}_{,\tau} = C_1\tilde{\Pi}_{,x} + A_1\hat{\Pi}_{,x} + \frac{C_\alpha}{sg}\tilde{\Pi} - \left(l+1+\frac{C_a}{sg}\right)\hat{\Pi}, \tag{31}$$

$$\mathring{\Pi}_{,\tau} = \frac{a}{g}\tilde{\Pi} - sxa\hat{\Pi} - l\mathring{\Pi}. \tag{32}$$

This is of the form $u_{,\tau} = Au_{,x} + Bu$, where the coefficients of the 2×2 matrix A are

$$A_1 = -x, \qquad B_1 = \frac{1}{sg}, \qquad C_1 = \frac{1}{sg}. \tag{33}$$

The matrix A has therefore the eigenvalues

$$\lambda_{1\pm} = -x \pm \frac{1}{sg}. \tag{34}$$

We have used GD1, GD2 and CD3. All three codes have numerical modes that are not physical. Often it is clear that they are related to weak modes at the light cone, and they can be discarded by inspection. Weak modes are particularly easy to spot in GD1, as it is the most causal code. In the other codes, the numerical counterparts of weak modes can appear quite smooth. In GD1 we can suppress weak modes completely by rearranging the grid spacing so that the light cone falls exactly on a grid point, and then truncating the grid at that point. This code will be referred to as GD1LC. In the other codes we need to pick out the physical modes by the criterion of convergence both with resolution for a single code and between different codes. Figure 5 demonstrates convergence of λ for the case $\kappa = 1/3$ and $l = 2$. The best values (either from GD2 or CD3) for the Lyapunov exponents are plotted as a function of κ and l in Fig. 6. The $l = 2$ leading mode is unstable for $0.58 \lesssim \kappa \lesssim 0.87$ (see also Fig. 7).

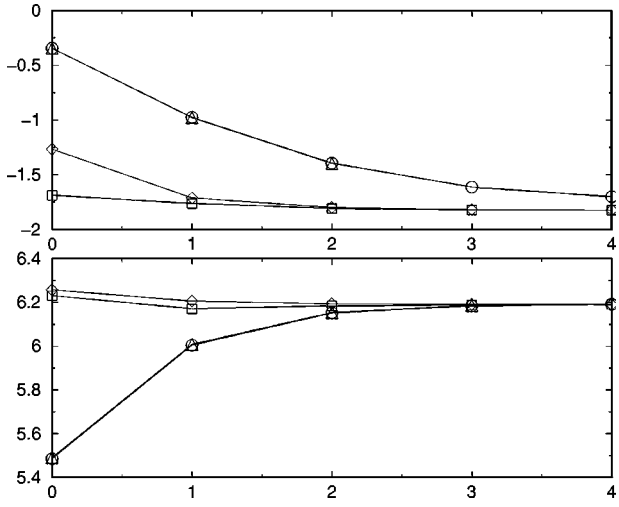

FIG. 5. Convergence of λ for the top physical $l=2$ axial (Π only) mode with resolution, at $\kappa = 1/3$. The upper graph is $\mathrm{Re}\,\lambda$, and the lower graph is $\mathrm{Im}\,\lambda$. From left to right $N = 10, 20, \ldots 160$. Circles are GD1, squares are GD1LC, diamonds GD2 and triangles up CD3.

Convergence tests fail to identify any mode as physical at the highest available resolution for $\kappa = 0.05$ at $l = 4$ and $\kappa = 0.1$ at $l = 5$. However, all modes of all three codes decay for these values of κ and l, so that we are fairly certain that there are no physical growing modes for these values of κ and l. Furthermore, for all κ, $\mathrm{Re}\,\lambda$ decreases with increasing l (see Fig. 6). Therefore we conclude that all $l \geqslant 3$ modes are stable.

E. Polar $l=1$ perturbations

In this section, we discuss the equations of motion for the $l=1$ (dipole) polar perturbations. There are no dipole gravitational waves, and therefore the gravitational field has no degrees of freedom independently of the matter. There are three matter degrees of freedom. They are an azimuthal fluid velocity perturbation α, a radial fluid velocity perturbation γ, and a density perturbation ω. (For the equation of state we use here, the pressure and density perturbations are related by $\delta p = \kappa\delta\rho$.) The metric perturbations are obtained from

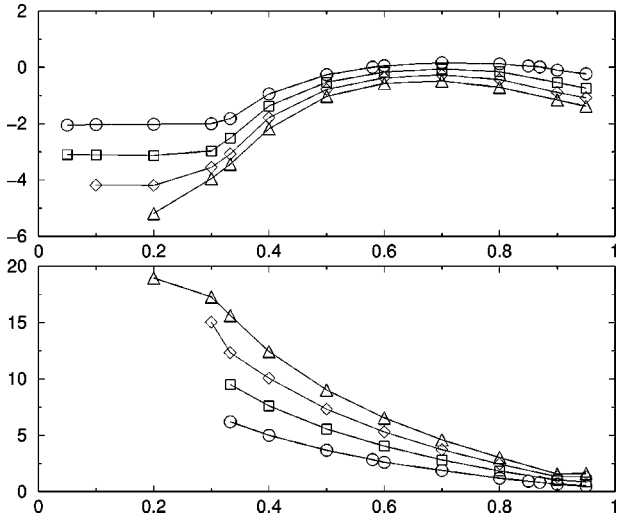

FIG. 6. Best value (using CD4) for the Lyapunov exponent λ of Π, against κ and l. The upper graph shows $\mathrm{Re}\,\lambda$ against κ, and the lower graph $\mathrm{Im}\,\lambda$. Circles denote $l=2$, squares $l=3$, diamonds $l=4$ and triangles $l=5$. Points are linked by straight lines. The points $\kappa=0.05,0.1$, $l=5$ and $\kappa=0.05$, $l=4$ are missing because λ could not be computed. The curves for $\mathrm{Im}\,\lambda$ end at small κ where the modes become real.

the matter perturbations by constraints. For a general discussion we refer the reader to [9]. Here we only carry out the reduction of the equations given there to a self-similar background solution.

We use the matter variables

$$\mathring{\alpha}\equiv r^{-1}\alpha, \qquad \mathring{\gamma}\equiv -(1+\kappa)\gamma, \qquad \mathring{\omega}\equiv\omega. \tag{35}$$

The matter perturbations are regular at the center if $\mathring{\alpha}$ and $\mathring{\gamma}$ are $O(1)$ and even in powers of x, and $\mathring{\omega}$ is $O(x)$ and odd. The leading orders of α and γ are additionally constrained as $(1+\kappa)\mathring{\alpha}+\mathring{\gamma}=O(x^2)$.

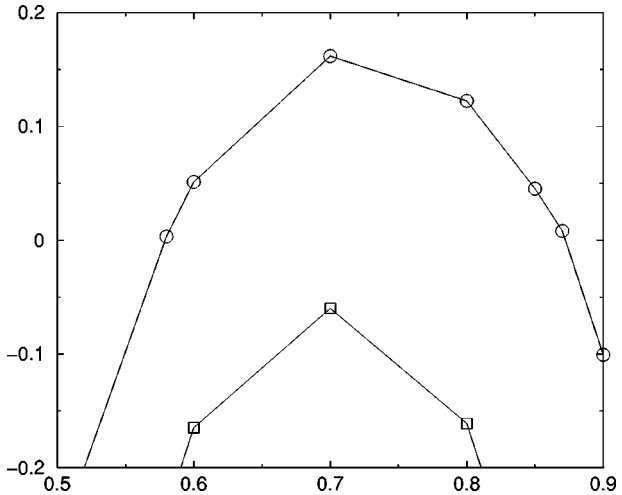

FIG. 7. Detail from Fig. 6 showing $\mathrm{Re}\,\lambda$ for $l=2$ and $l=3$. The $l=2$ leading mode is unstable for $0.58<\kappa<0.87$.

The perturbation variables are not completely gauge-invariant for $l=1$. We fix most of the gauge freedom by setting the metric perturbation $k=0$. In this (partially fixed) gauge the remaining metric perturbations ψ, χ and η are determined by constraints. We introduce suitably rescaled metric perturbation variables

$$\mathring{\chi}\equiv e^{-3\tau}r^{-3}\chi, \qquad \mathring{\psi}=e^{-2\tau}r^{-2}\psi, \qquad \mathring{\eta}=e^{-\tau}r^{-1}\eta. \tag{36}$$

The metric perturbations are regular at the center if $\mathring{\chi}$, $\mathring{\eta}$ and $\mathring{\psi}$ are all $O(1)$ and even in x. The perturbed spacetime is CSS if and only if all perturbations are independent of τ.

From Eqs. (99), (100) of [9], the equations of motion of the matter perturbations are

$$\dot{\mathring{\gamma}}-\kappa\mathring{\omega}'=-\overline{S}_\gamma \tag{37}$$

$$\dot{\mathring{\omega}}-\mathring{\gamma}'=-\overline{S}_\omega \tag{38}$$

$$\dot{\mathring{\alpha}}=-r^{-1}S_\alpha-U\mathring{\alpha}, \tag{39}$$

where the expressions $\overline{S}_\gamma$, $\overline{S}_\omega$ and S_α are given by Eqs. (A9)–(11) of [9]. The first two equations constitute a first-order form of a wave equation whose characteristics have velocity $\sqrt{\kappa}$ with respect to the background fluids: they describe sound waves. The third equation transports $\mathring{\alpha}$ along the fluid. Solving the three matter equations for the τ derivatives, on a continuously self-similar background spacetime, one obtains the following system of evolution equations:

$$\mathring{\gamma}_{,\tau}=A_\kappa\mathring{\gamma}_{,x}+B_\kappa\mathring{\omega}_{,x}+S(\mathring{\gamma}), \tag{40}$$

$$\mathring{\omega}_{,\tau}=C_\kappa\mathring{\gamma}_{,x}+A_\kappa\mathring{\omega}_{,x}+S(\mathring{\omega}), \tag{41}$$

$$\mathring{\alpha}_{,\tau}=F\mathring{\alpha}_{,x}+S(\mathring{\alpha}). \tag{42}$$

The coefficients of the 3×3 matrix A in Eq. (24) are

$$A_\kappa=-x-\frac{(1-\kappa)V}{(1-\kappa V^2)sg}, \qquad B_\kappa=\frac{\kappa(1-V^2)}{(1-\kappa V^2)sg},$$

$$C_\kappa=\frac{(1-V^2)}{(1-\kappa V^2)sg}, \qquad F=-x-\frac{V}{sg}. \tag{43}$$

Its eigenvalues, the characteristic speeds, are

$$\lambda_{\kappa\pm}=-x-\frac{(1-\kappa)V}{(1-\kappa V^2)sg}\pm\frac{\sqrt{\kappa}(1-V^2)}{(1-\kappa V^2)sg}, \quad \lambda_0=-x-\frac{V}{sg}. \tag{44}$$

The constraint equations for the metric perturbations are also given in [9]. The derivative operator D becomes a simple partial derivative in coordinates x and τ, namely $rD=x\partial/\partial x$. We obtain a system of three ODEs in x, from now on referred to as the constraints:

$$xu_{,x}=Mu+s, \quad u=(\overset{\circ}{\chi},\overset{\circ}{\eta},\overset{\circ}{\psi}). \tag{45}$$

M and s are given in Appendix B.

We now return to the issue of the gauge freedom that is left after one has set $k=0$. The change of k under an arbitrary gauge transformation parametrized by the variable $\overset{\circ}{\xi}$ is $\overset{\circ}{k}\to\overset{\circ}{k}+L_1\overset{\circ}{\xi}$ (see [9] for details). L_1 is a differential operator (roughly speaking a second x derivative), whose kernel is parametrized by one free function of τ. The remaining gauge freedom can therefore be fixed by imposing a gauge condition worth one function of τ. There are two natural choices. In "η gauge" we set $\overset{\circ}{\eta}=O(x^2)$ at the center. In "α gauge" we set $\overset{\circ}{\alpha}=O(x^2)$, and therefore also $\overset{\circ}{\gamma}=O(x^2)$. Numerically it is not easy to enforce that any variable behaves as $O(x^2)$ at the center. Therefore we impose the two sub-gauges using variables rescaled by suitable powers of x. This is discussed in Appendix B.

Although by function counting either α gauge or η gauge should fix the residual gauge freedom in $k=0$, a single gauge mode does in fact survive in each gauge. The change of $\overset{\circ}{\eta}$ under a gauge transformation is $\overset{\circ}{\eta}\to\overset{\circ}{\eta}+L_2\overset{\circ}{\xi}$. Any residual $\overset{\circ}{\xi}$ must now obey both $L_1\overset{\circ}{\xi}=0$, from the gauge condition $k=0$, and $L_2\overset{\circ}{\xi}=O(x^2)$, from the gauge condition $\overset{\circ}{\eta}=O(x^2)$, where L_2 is another differential operator (roughly speaking the wave operator). A careful calculation shows that the two joint equations still have one non-zero solution, which is $\overset{\circ}{\xi}_0=e^{\lambda\tau}f(x)$ for

$$\lambda=\frac{1}{2}\pm i\sqrt{\left(\kappa+\frac{1}{3}\right)\overline{\rho}(0)-\frac{1}{4}}. \tag{46}$$

That means that in the $\eta=O(x^2)$ sub-gauge of the $k=0$ gauge we have a single complex conjugate pair of gauge modes left.

The situation is similar in α gauge: The change of $\overset{\circ}{\alpha}$ under a gauge transformation is $\overset{\circ}{\alpha}\to\overset{\circ}{\alpha}+L_3\overset{\circ}{\xi}$ for some operator L_3, roughly speaking a first τ derivative. The joint kernel of $L_1\overset{\circ}{\xi}=0$ and $L_3\overset{\circ}{\xi}=O(x^2)$ is not empty either but contains a single real gauge mode with

$$\lambda=\frac{1+3k}{3(1+k)}. \tag{47}$$

Both gauge modes are in fact found numerically, and give us a check on the numerical precision for each value of κ. Figure 8 demonstrates this for both gauges.

We have used GD1, GD2 and CD4. For $\kappa\gtrsim 0.15$, the numerical results are straightforward. Both in α gauge and in η gauge, we find the expected gauge mode. We find that α gauge, in the specialized variables described in Appendix B, has the best numerical behavior at the center. As an estimate of numerical error in the code, Fig. 9 shows the exact and numerical value of λ for the gauge mode in α gauge. Figure 10 shows the best value of λ in this system as a function of κ.

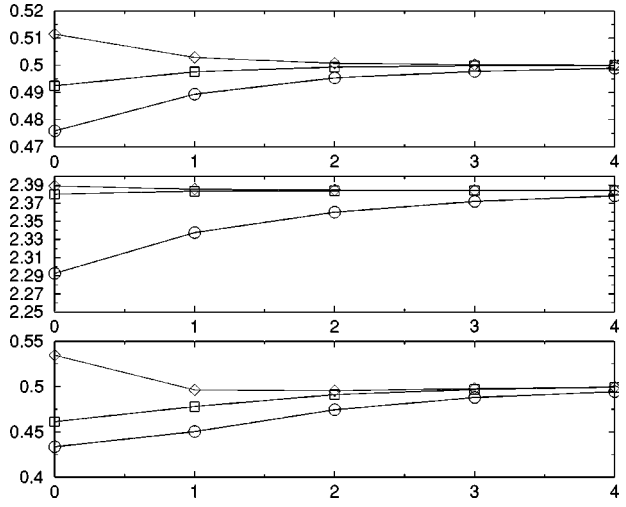

FIG. 8. Convergence of λ for the single gauge mode in the $l=1$ polar perturbations, for $\kappa=1/3$. From left to right $N=10,20,\ldots 160$. Circles are GD1, squares are GD2, and diamonds CD4. The top two graphs were obtained in η gauge, using the variables of Appendix A, and show $\mathrm{Re}\,\lambda$ and $\mathrm{Im}\,\lambda$ for the gauge mode. The value of λ for this mode computed from the background solution and Eq. (46) is $\lambda\simeq 1/2+2.384i$ for $\kappa=1/3$. The bottom graph was obtained in α gauge, using the variables described in Appendix B. The exact value of λ for this gauge mode is 1/2 for $\kappa=1/3$.

For $\kappa\lesssim 0.15$, our code does not work well. Figure 9 shows that with decreasing κ, the error in locating the gauge mode increases rapidly. For $\kappa=0.1$ and $\kappa=0.05$, all three codes fail to find the real gauge mode. Nevertheless, GD1 and GD2 have precisely one growing mode, and CD4 has precisely one growing mode that is not clearly a grid mode. All these modes are complex, but they obey $|\mathrm{Re}\,u(x)|\gg|\mathrm{Im}\,u(x)|$ for all x, by a factor of ~ 100: the mode is al-

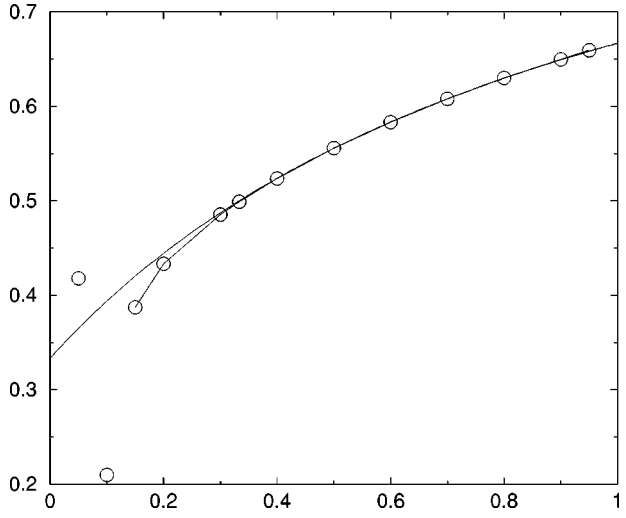

FIG. 9. λ for the single gauge mode in the $l=1$ polar perturbations in α gauge as a function of κ. Circles are measured values, connected by straight lines. The smooth curve is the exact value. The points at $\kappa=0.1$ and $\kappa=0.05$ represent the real part of the only growing mode present, which is complex.

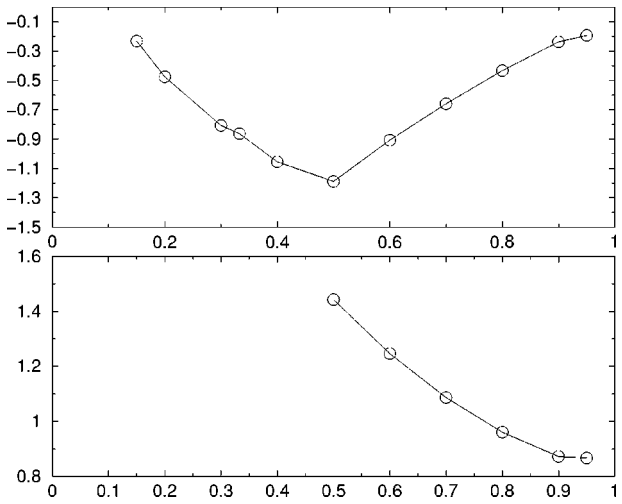

FIG. 10. Best value (obtained with GD2) for the physical Lyapunov exponent λ of the $l=1$ polar perturbations. The upper graph shows Re λ against κ, and the lower graph Im λ. Points are connected by straight lines. The measured values end at $\kappa=0.15$ because for $\kappa=0.1$ and $\kappa=0.05$ the top mode could not be identified. The graph of Im λ ends because λ is real for $\kappa<0.5$. Clearly a real mode and a complex mode pair have crossed between $\kappa=0.5$ and $\kappa=0.6$.

most real, modulated by a $\cos\omega\tau$ factor. It is also clear that there is a finite differencing problem at the center that affects all three codes: the functions $u(x)$ are not well-behaved even or odd functions. The origin of this instability is uncertain. A plausible explanation is that the numerical background solution itself is not sufficiently well-behaved at the center for small κ. Some of the coefficients in the $l=1$ (and also $l\geqslant 2$) polar perturbation equations are very large and sharply peaked at the center. Furthermore, some of these coefficients must be obtained as numerical derivatives of the background solution. These numerical derivatives are not smooth at the center, and we had to artificially extrapolate them to the center in order to smoothe them.

Because all three codes agree on a single growing mode that is almost real in the sense just defined, we identify this mode with the gauge mode, even though the agreement in λ is poor. This leaves no other growing modes in any of the codes for any κ (except for obvious grid modes in CD4 that can be ruled out by inspection.) We therefore conjecture that there are no growing physical modes, even though we cannot identify the top physical mode.

F. Polar $l\geqslant 2$ perturbations

As discussed in detail in [9], the $l\geqslant 2$ polar perturbations of a spherical perfect fluid admit a free evolution formulation. The dynamical variables that can be specified freely are the metric perturbations χ, k and ψ, and the time derivatives $\dot{\chi}$ and $\dot{k}$. χ and k obey wave equations, and ψ a transport equation, all of which are coupled. There are three gauge-invariant matter perturbations. α is an azimuthal velocity perturbation, γ is a radial velocity perturbation, and ω is a pressure and density perturbation. These matter perturbation variables are completely determined as algebraic expressions in the seven first-order metric perturbation variables, as discussed in detail in [9]. For the purpose of finding the late-time behavior of generic perturbations, we work with the metric perturbations alone.

Solving for the τ derivative of the seven variables, we find that the matrix A in Eq. (24) takes the following form:

$$A=\begin{pmatrix} A_1 & B_1 & & & D \\ C_1 & A_1 & & & VD \\ & & A_\kappa & B_\kappa & E \\ & & C_\kappa & A_\kappa & VE \\ & & & & F \end{pmatrix}, \quad u=\begin{pmatrix} \tilde{\chi} \\ \hat{\chi} \\ \tilde{k} \\ \hat{k} \\ \mathring{\psi} \end{pmatrix}. \tag{48}$$

The remaining two variables $\mathring{\chi}$ and $\mathring{k}$ are evolved using only source terms. The coefficients of the matrix A have already been given in Eqs. (33) and (43), except for

$$D=\frac{2(\bar{\mu}-\bar{U})}{s^2 gx}, \quad E=-\frac{2\kappa x\bar{U}(1-V^2)}{(1-\kappa V^2)g}. \tag{49}$$

The five eigenvalues of A are $\lambda_{1\pm}$, $\lambda_{\kappa\pm}$ and λ_0, which have already been given. (D and E do not influence the eigenvalues.) Note that s has been chosen so that $\lambda_{\kappa+}>0$ for $0\leqslant x<1$. The point $x=1$ where it changes sign is the sound cone. Similarly, the point $x=x_{\rm lc}>1$ where λ_{1+} changes sign is the light cone. Clearly $x_{\rm lc}$ is 1 for $\kappa=1$ and diverges as $\kappa\to 0$. Note that the $(\tilde{\chi},\hat{\chi})$ submatrix of A is the same as the entire matrix A for the axial Π perturbations, as both pairs of variables obey a wave equation at the speed of light. Similarly, the $(\tilde{k},\hat{k})$ submatrix is equal to the entire matrix for the $l=1$ polar perturbations, which obey a wave equation at the speed of sound. Therefore A_κ is equal to A_1 for $\kappa=1$, when the speed of sound is the speed of light.

We have used the three codes GD1, GD2 and CD3. There is good agreement and convergence between the three codes for $0.2\lesssim\kappa\lesssim 0.8$. Figure 11 demonstrates convergence of λ for $\kappa=1/3$ and $l=2$. Figure 12 shows the best values of λ for $l=2\ldots 5$. We find that all modes for all l decay for $\kappa\lesssim 0.49$. For $\kappa\gtrsim 0.49$, there is an unstable $l=2$ mode (see Fig. 13). At still higher κ, there is probably more than one unstable mode, but it is difficult to identify subdominant modes with certainty.

For $\kappa\gtrsim 0.8$, and $\kappa\lesssim 0.2$, the numerical precision decreases quickly. In this region the numerical accuracy is poor for $l=2$, and for $l=3,4,5$ even the top physical mode cannot be identified clearly. The origin of these problems is different for high and low κ. At high κ, all modes in all three codes show discontinuities at the sound cone. These are not due to the weak modes discussed above, but are due to unsmooth behavior in the numerical background solution, through certain coefficients of the perturbation equations that must be obtained as numerical derivatives of the background solution. At low κ, the origin of the low precision is not so clear. It may be that the background coefficients become increas-

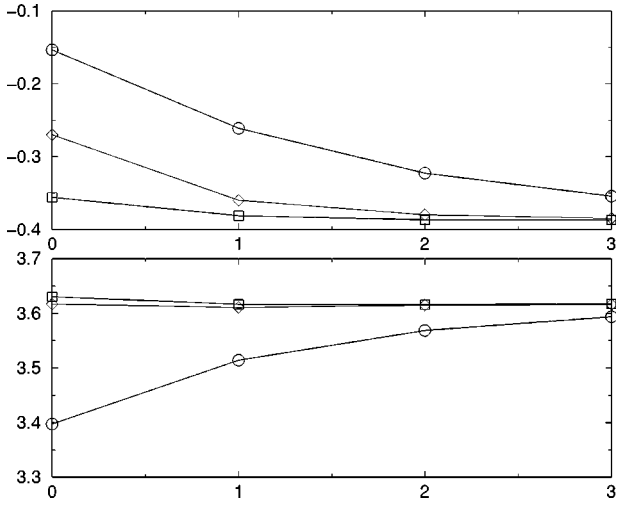

FIG. 11. Convergence of λ for the top $l=2$ polar mode with resolution at $\kappa=1/3$. From left to right $N=20,40,\ldots 160$. Circles are GD1, squares are GD2, and diamonds CD3. The upper graph is Re λ, and the lower graph is Imλ.

ingly large and sharply peaked in x near the center as $\kappa \to 0$. With the sound cone at $x=1$, the value of x at the light cone also diverges as $1/\sqrt{k}$ as the sound speed goes to zero. (Recall that x is defined so that the sound cone is at $x=1$.) In a second source of error, some of the perturbation coefficients, as determined from the numerical background solution, must be smoothed at the center for small κ, and this introduces additional error. (This is the same problem that affects the $l=1$ polar modes.)

In contrast to the inadequacy of the numerics at high and low κ, the numerical precision is good in a large neighborhood of the value $\kappa \simeq 0.49$. It is therefore certain that the $l=2$ polar perturbations are stable for $\kappa \lesssim 0.49$ and unstable

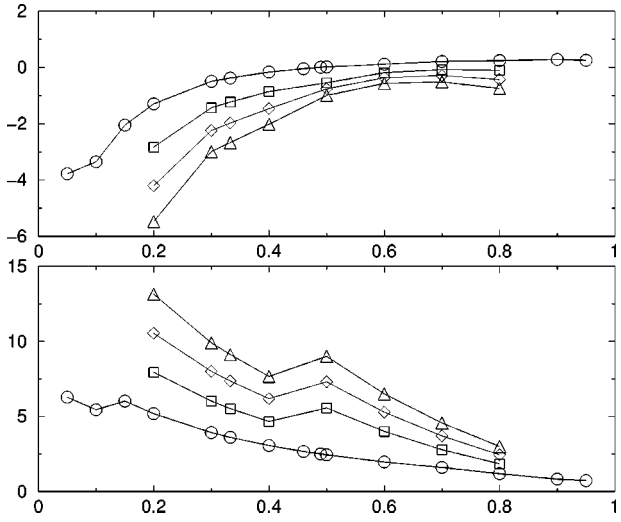

FIG. 12. λ for the top $l=2\ldots5$ polar modes as a function of κ. The upper graph is Re λ, and the lower graph is Im λ. Circles are $l=2$, squares $l=3$, diamonds $l=4$ and triangles $l=5$. Note that Re λ decreases with l, while Im λ increases. The curves for $l=3,4,5$ do not extend to the lowest and highest κ because of large numerical error.

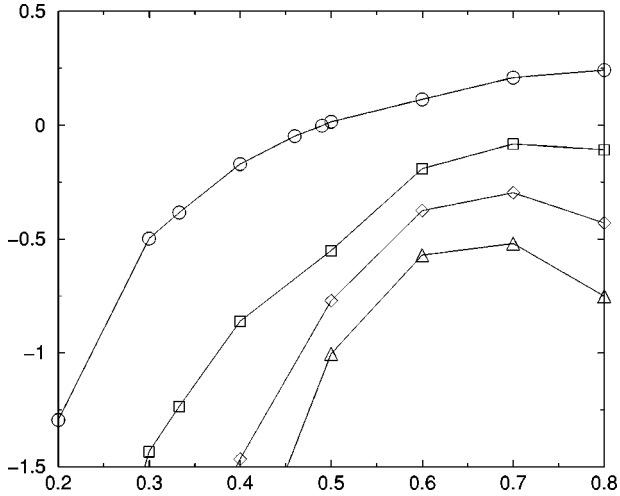

FIG. 13. Detail of Fig. 12. Re λ is positive for $l=2$, $\kappa>0.49$. Re λ is negative for all κ for $l>2$.

for $\kappa \gtrsim 0.49$. As evidence that the instability is physical, Fig. 14 demonstrates the convergence of independent residual evaluations between all three codes for $l=2$ and $\kappa=0.6$. From convergence, we estimate λ (for this κ and l) as $\lambda = (0.112 \pm 0.003) + (1.968 \pm 0.005)i$. The real part of λ is therefore much larger than the finite differencing error.

V. CONCLUSIONS

The threshold of gravitational collapse of a perfect fluid with $p=k\rho$ in spherical symmetry shows ''type II'' critical

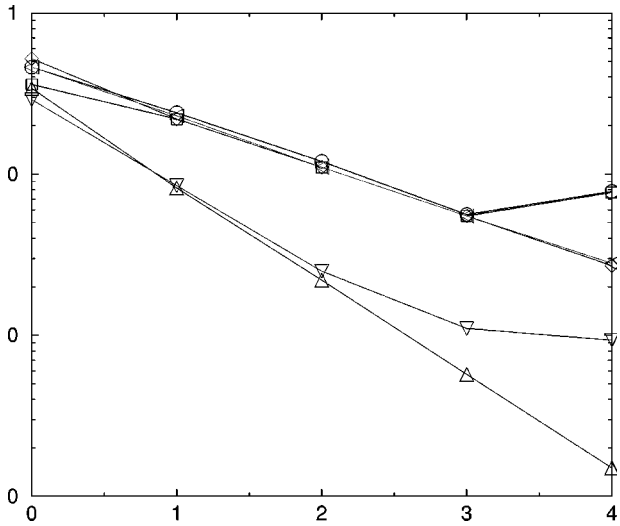

FIG. 14. Log-log plot of independent residual evaluation between three different codes for the dominant polar $l=2$ mode for $\kappa=0.6$. Evaluating the mode produced by GD2 with CD3 shows exact second-order convergence (triangles up, bottom curve). The opposite operation, checking on CD3 with GD2, shows second-order convergence that breaks down at high resolution (triangles down). Checking on CD3 and GD2 with GD1 shows the expected first-order convergence (triangles left and diamonds). The opposite check shows first-order convergence that breaks down at high resolution (squares and circles, top curves). The resolutions shown are $\Delta x=1/10\ldots1/160$.

phenomena (including mass scaling with a critical exponent) for the entire range $0<k<1$ [4–7]. Is this true also when one relaxes the assumption of spherical symmetry? We have addressed this question by studying the nonspherical perturbations of the critical solutions in spherical symmetry. We have extended the results of [8] from $\kappa=1/3$ in the equation of state $p=k\rho$ to the entire physical range $0<k<1$. Because of the numerical difficulties, we have complemented the single first-order scheme used in [8] with three different second-order finite differencing schemes. We have complemented convergence tests by independent residual evaluation. This allows us to identify ''weak modes,'' numerical artifacts related to weak solutions of the perturbation equations. Finally, we have corrected errors in [8] concerning the equations of motion for the $l=1$ axial and polar perturbations.

After verifying that the CSS solution has exactly one growing spherical perturbation for all κ, we have found that all nonspherical perturbations decay for all κ with the following exceptions:

(1) For $\kappa<1/9$, there is precisely one growing $l=1$ axial mode. This result was obtained analytically, even though the background solution is known only numerically. Because it is $l=1$, this mode is three-fold degenerate.

(2) For $\kappa\gtrsim 0.49$, there is a growing $l=2$ polar mode. We cannot rule out that at larger κ, there are several growing modes. Because it is $l=2$, this mode is five-fold degenerate.

(3) For $0.58\lesssim\kappa\lesssim 0.87$, there is also a growing $l=2$ axial mode.

The numerical evidence for this is not as good as one would like. Because of numerical error, we cannot measure λ of the top physical mode of the $l=1$ polar perturbations for $\kappa\lesssim 0.15$, nor of the $l\geqslant 3$ polar perturbations for $\kappa\lesssim 0.2$ and $\kappa\gtrsim 0.8$. However, in all these cases where physical modes and numerical modes cannot be distinguished clearly, all modes, including the physical modes, do in fact decay. Therefore we still argue that all physical modes, apart from those enumerated above, decay. One cause of the numerical difficulty is the separate existence of light cones and sound cones, which gives rise to numerical artifacts related to weak solutions of the continuum equations. A second cause is that instead of a single smooth background solution we are dealing with a one-parameter family of such solutions, which is ill-behaved at both ends $\kappa=0$ and $\kappa=1$. A third cause is that several coefficients required in the perturbation equations are first and second derivatives of the background fields, which are not perfectly smooth at the center and the light cone.

What is the significance of our results? The $l=1$ axial perturbations are naturally associated with infinitesimal (differential) rotation. The presence of a growing rotation mode at low κ ($<1/9$) is not surprising, as one would expect a rotating dust configuration to be torn apart by centrifugal forces. For a sufficiently stiff fluid this intuition obviously fails. The significance of the $l=1$ axial perturbations is that they can survive into the final black hole formed in collapse (and turn a Schwarzschild black hole into a Kerr black hole), while all other non-spherical perturbations must be radiated during collapse. Their instability is expected to give rise to interesting new phenomena in critical collapse that will be explored elsewhere [13].

The existence of a small number of unstable polar modes at high κ ($\gtrsim 0.49$) is more puzzling. At face value it suggests that the spherically symmetric CSS solution is a critical solution only when restricted to exact spherical symmetry. Its place may be taken by another critical solution with less symmetry, or there may not be a critical solution, and hence no universality, at the black hole threshold.

ACKNOWLEDGMENTS

I am grateful to José M. Martín-García for pointing out that I was using the wrong equations of motion for $l=1$ perturbations in [8], and for help in correcting them. I would like to thank Bob Wald for helpful conversations on the $l=1$ axial perturbation equation, and Miguel Alcubierre, Matt Choptuik, Giampaolo D'Alessandro and David Garfinkle for suggestions on numerical methods. This research was supported in part by NSF grant PHY-95-14726 to the University of Chicago, and by EPSRC grant GR/N10172.

APPENDIX A: BACKGROUND EQUATIONS

The relation between the fluid frame derivatives and the partial derivatives in CSS coordinates is

$$\dot{f}=\frac{e^{\tau}g}{a\sqrt{1-V^2}}\left[f_{,\tau}+\left(x+\frac{V}{sg}\right)f_{,x}\right], \tag{A1}$$

$$f'=\frac{e^{\tau}g}{a\sqrt{1-V^2}}\left[Vf_{,\tau}+\left(Vx+\frac{1}{sg}\right)f_{,x}\right], \tag{A2}$$

$$rDf=xf_{,x}. \tag{A3}$$

The perturbation equations of [9] allow for a 2-parameter equation of state $p=p(\rho,s)$, where s is the entropy per particle. When restricting to our simple baryotropic equation of state, we set both the fluid entropy s and its gauge-invariant perturbation σ to zero. We also set $C\equiv\partial p/\partial s$ to zero, and we set the sound speed squared $c_s^2\equiv\partial p/\partial\rho$ equal to the constant κ.

The background equations that result from the CSS ansatz are

$$a^{-2}=1-\frac{2s^2x^2\overline{\rho}}{1-V^2}\left[1+\kappa V^2+\frac{(1+\kappa)V}{sgx}\right] \tag{A4}$$

$$\frac{d\ln\overline{\rho}}{dx}=(1+\kappa)D^{-1}[(V+gsx)S_1-(1+Vgsx)S_2], \tag{A5}$$

$$\frac{dV}{dx}=(1-V^2)D^{-1}[-\kappa(1+Vgsx)S_1+(V+gsx)S_2], \tag{A6}$$

$$x\frac{d\ln g}{dx}=1-a^2+(1-\kappa)x^2s^2a^2\overline{\rho}, \tag{A7}$$

where

$$S_1\equiv 2\frac{V}{x}+\frac{2gs}{1+\kappa}+VC_\alpha+C_a, \tag{A8}$$

$$S_2\equiv \frac{2\kappa Vgs}{1+\kappa}+C_\alpha+VC_a, \tag{A9}$$

$$D\equiv\kappa(1+Vgsx)^2-(V+gsx)^2, \tag{A10}$$

$$C_a\equiv\frac{ra_{,t}}{x\alpha}=-xs^2\overline{\rho}a^2(1+\kappa)\frac{V}{1-V^2}=O(x^2), \tag{A11}$$

$$C_\alpha\equiv\frac{r\alpha_{,r}}{x\alpha}=\frac{a^2-1}{2x}+s^2x\overline{\rho}a^2\left(\frac{1+\kappa}{1-V^2}-1\right)=O(x). \tag{A12}$$

Here Eqs. (A5) and (A6) are the fluid equations of motion, and Eqs. (A7) and (A4) are two of the Einstein equations. The terms C_a and C_α arise when metric derivatives in the matter equations are eliminated using the Einstein equations. The expression for a incorporates the regularity condition (absence of a conical singularity) $a=1$ at $r=0$.

The following background quantities are required as coefficients in the perturbation equations:

$$\overline{W}\equiv e^{-\tau}W\equiv e^{-\tau}n^Ar_{,A}=(asx)^{-1}(1-V^2)^{-1/2}=O(x^{-1}), \tag{A13}$$

$$\overline{U}\equiv e^{-\tau}U\equiv e^{-\tau}u^Ar_{,A}=V\overline{W}=O(1),$$

$$\overline{\mu}\equiv e^{-\tau}\mu\equiv e^{-\tau}u^A{}_{|A}=O(1),$$

$$\overline{\nu}\equiv e^{-\tau}\nu\equiv e^{-\tau}n^A{}_{|A}=O(x), \tag{A14}$$

$$\overline{\rho}\equiv e^{-2\tau}4\pi\rho=O(1),$$

$$\frac{2m}{r}\equiv 1-r_{,A}r^{,A}=1-r^2(W^2-U^2)=1-a^{-2}=O(x^2). \tag{A15}$$

In a CSS background all these quantities depend only on x, and we have indicated their behavior at the origin.

APPENDIX B: $l=1$ POLAR PERTURBATION EQUATIONS

The source terms in Eq. (40) are obtained from the equations of [9] in the form

$$S(\mathring{\gamma})=-e^{-\tau}a\sqrt{1-V^2}g(1-\kappa V^2)(\overline{S}_\gamma+\kappa V\overline{S}_\omega), \tag{B1}$$

$$S(\mathring{\omega})=-e^{-\tau}a\sqrt{1-V^2}g(1-\kappa V^2)(V\overline{S}_\gamma+\overline{S}_\omega), \tag{B2}$$

$$S(\mathring{\alpha})=-e^{-\tau}a\sqrt{1-V^2}g(r^{-1}S_\alpha+U\mathring{\alpha}), \tag{B3}$$

where the terms on the right-hand side are defined in Ref. [9]. Fully expanded in the variables adapted to self-similarity, they are

$$S(\mathring{\gamma})=\frac{a\sqrt{1-V^2}}{g(1-\kappa V^2)}\left\{[(\kappa-1)\overline{\mu}+4\kappa\overline{U}+(\kappa-1)V\overline{\nu}]\mathring{\gamma}-2\kappa(1+\kappa)V\left[-\frac{1}{sx}+(1+\kappa)sx\overline{\rho}\right]\mathring{\alpha}\right.$$
$$\left.+\frac{1}{2}(1+\kappa)^2(\overline{\mu}+V\overline{\nu})(sx)^2\mathring{\psi}-(1+\kappa)[\overline{\nu}-\overline{W}+\kappa V(\overline{\mu}+U)](sx)\mathring{\eta}+(1+\kappa)(\overline{\nu}+\kappa V\overline{\mu})(sx)^3\mathring{\chi}\right\}, \tag{B4}$$

$$S(\mathring{\omega})=\frac{a\sqrt{1-V^2}}{g(1-\kappa V^2)}\left\{\left[(\kappa-1)V\overline{\mu}+2\kappa V\overline{U}+\frac{\kappa-1}{\kappa}\overline{\nu}+2\overline{W}\right]\mathring{\gamma}-2(1+\kappa)\left[-\frac{1}{sx}+(1+\kappa)sx\overline{\rho}\right]\mathring{\alpha}\right.$$
$$\left.+\frac{1}{2}(1+\kappa)\left(\frac{1+\kappa}{\kappa}\overline{\nu}-2\overline{W}+(1+\kappa)V\overline{\mu}+2\kappa V\overline{U}\right)(sx)^2\mathring{\psi}-(1+\kappa)(\overline{\mu}+V\overline{\nu})(sx)\mathring{\eta}+(1+\kappa)(\overline{\mu}+V\overline{\nu})(sx)^3\mathring{\chi}\right\}, \tag{B5}$$

$$S(\mathring{\alpha})=\frac{a\sqrt{1-V^2}}{g}\left\{-\frac{\kappa}{1+\kappa}(sx)^{-1}\mathring{\omega}+[\kappa\overline{\mu}+(2\kappa-1)\overline{U}]\mathring{\alpha}-\mathring{\eta}+\frac{1}{2}(sx)^2\mathring{\chi}\right\}. \tag{B6}$$

The coefficients in the constraint equations (45) are

$$M=\begin{pmatrix} -1+a^2[-2+(1-\kappa)(sx)^2\overline{\rho}] & a^2(4\overline{U}\overline{W}+2\overline{\mu}\overline{W}-2\overline{\nu}\overline{U})(sx) & 2a^2(\overline{\nu}\overline{U}-\overline{\mu}\overline{W})(sx)^3 \\ -2a^2\overline{U}\overline{W}(sx)^3 & 2-2a^2[1-\overline{U}^2(sx)^2+\kappa\overline{\rho}(sx)^2] & -a^2[\overline{W}^2+\overline{U}^2-(1+\kappa)\overline{\rho}](sx)^4 \\ 2a^2[\overline{U}\overline{\nu}-(\overline{\mu}+\overline{U})\overline{W}](sx) & -2a^2\overline{U}^2 & -3-2a^2[1+\overline{U}^2(sx)^2-(sx)^2\overline{\rho}] \end{pmatrix} \tag{B7}$$

$$s=a^2(-2\overline{\rho}\mathring{\gamma}+4\overline{\rho}(1+\kappa)\overline{W}(sx)\mathring{\alpha},\quad (1-\kappa)\overline{\rho}(sx)\mathring{\omega}-4(1+\kappa)\overline{\rho\overline{U}}(sx)^2\mathring{\alpha},\quad 2\overline{\rho}(sx)^{-1}\mathring{\omega}-8(1+\kappa)\overline{\rho\overline{U}\alpha}). \tag{B8}$$

In "η gauge" we set $\mathring{\eta}=O(x^2)$ at the center. The constraint equations are then solved with the boundary conditions

$$\mathring{\psi}=2(1+\kappa)\overline{\rho\alpha},\quad \mathring{\eta}=0,\quad \mathring{\chi}=\frac{2}{5}\overline{\rho}(sx)^{-1}\mathring{\omega}+\frac{32}{15}\overline{\rho\alpha} \tag{B9}$$

at the center $x=0$. The condition $\mathring{\eta}=0$ is our gauge condition, and the other two conditions follow from $Mu+s=0$ (M has rank 2 at the center). An alternative way of imposing η gauge is to introduce the new variable

$$\tilde{\eta}=(sx)^{-2}\mathring{\eta}, \tag{B10}$$

which is $O(1)$ at the center in this gauge. The evolution equations are as before, with only $\mathring{\eta}$ replaced by $(sx)^2\tilde{\eta}$ in Eqs. (B4)–(B6). The constraint equations become

$$x\tilde{u}_{,x}=\tilde{M}\tilde{u}+\tilde{s},\quad \tilde{u}=(\mathring{\chi},\tilde{\eta},\mathring{\psi}), \tag{B11}$$

with

$$\tilde{M}=\begin{pmatrix} -1+a^2[-2+(1-\kappa)(sx)^2\overline{\rho}] & a^2(4\overline{U}\overline{W}+2\overline{\mu}\overline{W}-2\overline{\nu U})(sx)^3 & 2a^2(\overline{\nu U}-\overline{\mu}\overline{W})(sx)^3 \\ -2a^2\overline{U}\overline{W}sx & -2a^2[1-\overline{U}^2(sx)^2+\kappa\overline{\rho}(sx)^2] & -a^2[\overline{W}^2+\overline{U}^2-(1+\kappa)\overline{\rho}](sx)^2 \\ (2a^2[\overline{U\nu}-(\overline{\mu}+\overline{U})\overline{W}](sx) & -2a^2\overline{U}^2(sx)^2 & -3-2a^2[1+\overline{U}^2(sx)^2-(sx)^2\overline{\rho}] \end{pmatrix} \tag{B12}$$

$$\tilde{s}=a^2(-2\overline{\rho}\mathring{\gamma}+4\overline{\rho}(1+\kappa)\overline{W}sx\mathring{\alpha},\quad (1-\kappa)\overline{\rho}(sx)^{-1}\mathring{\omega}-4(1+\kappa)\overline{\rho\overline{U}}\mathring{\alpha},\quad 2\overline{\rho}(sx)^{-1}\mathring{\omega}-8(1+\kappa)\overline{\rho\overline{U}\alpha}). \tag{B13}$$

The boundary conditions at $x=0$ are

$$\mathring{\psi}=2\overline{\rho}(1+\kappa)\mathring{\alpha},\quad \tilde{\eta}=-\frac{1}{5}\overline{\rho}(sx)^{-1}\mathring{\omega}+\frac{4}{15}\overline{\rho}\mathring{\alpha},$$

$$\mathring{\chi}=\frac{2}{5}\overline{\rho}(sx)^{-1}\mathring{\omega}+\frac{32}{15}\overline{\rho}\mathring{\alpha}, \tag{B14}$$

from $Mu+s=0$ (M has rank 3 at the center).

In "α gauge" we set $\mathring{\alpha}=O(x^2)$ [and therefore also $\mathring{\gamma}=O(x^2)$]. The constraints are then solved with the boundary conditions

$$\mathring{\psi}=\frac{4\kappa}{3(1+\kappa)^2}(sx)^{-1}\mathring{\omega},\quad \mathring{\eta}=-\frac{\kappa}{1+\kappa}(sx)^{-1}\mathring{\omega},$$

$$\mathring{\chi}=\left(\frac{2}{5}\overline{\rho}+\frac{8\kappa}{9(1+\kappa)^3}\right)(sx)^{-1}\mathring{\omega}. \tag{B15}$$

Here the boundary condition on η comes from consistency with the evolution equation $\mathring{\alpha}_{,\tau}=O(x^2)$. An alternative way of imposing α gauge is to introduce new matter variables

$$\hat{\omega}\equiv(sx)^{-1}\mathring{\omega},\quad \hat{\gamma}\equiv\kappa^{-1}(sx)^{-1}\mathring{\gamma},\quad \check{\alpha}\equiv(sx)^{-1}\mathring{\alpha}=sx\hat{\alpha}. \tag{B16}$$

The evolution equations in these variables are

$$\hat{\omega}_{,\tau}=A_\kappa\hat{\omega}_{,x}+B_\kappa\hat{\gamma}_{,x}+S(\hat{\omega}), \tag{B17}$$

$$\hat{\gamma}_{,\tau}=C_\kappa\hat{\omega}_{,x}+A_\kappa\hat{\gamma}_{,x}+S(\hat{\gamma}), \tag{B18}$$

$$\check{\alpha}_{,\tau}=F\check{\alpha}_{,x}+S(\check{\alpha}). \tag{B19}$$

Note that the coefficients of the x derivatives are unchanged, but that $\hat{\omega}$ has taken the place of $\mathring{\gamma}$ and $\hat{\gamma}$ has taken the place of $\mathring{\omega}$. Accordingly, $\hat{\gamma}$ is now odd and $O(x)$ while $\hat{\omega}$ is even and $O(1)$. The source terms are

$$S(\hat{\gamma})=a\sqrt{1-V^2}\kappa g(1-\kappa V^2)\Big\{[(\kappa-1)\overline{\mu}+4\kappa\overline{U}+(\kappa-1)V\overline{\nu}]\kappa\hat{\gamma}-2\kappa(1+\kappa)V[-1+(1+\kappa)(sx)^2\overline{\rho}]\times(sx)^{-1}\check{\alpha}+\frac{1}{2}(1+\kappa)^2(\overline{\mu}+V\overline{\nu})sx\mathring{\psi}-(1+\kappa)$$

$$\times[\overline{\nu}-\overline{W}+\kappa V(\overline{\mu}+U)]\mathring{\eta}+(1+\kappa)$$
$$\times(\overline{\nu}+\kappa V\overline{\mu})(sx)^2\mathring{\chi}\Big\}$$
$$-\left[1+\frac{(1-\kappa)V}{(1-\kappa V^2)sgx}\right]\hat{\gamma}+\frac{1-V^2}{(1-\kappa V^2)sgx}\hat{\omega}, \quad \text{(B20)}$$

$$S(\hat{\omega})=a\sqrt{1-V^2}g(1-\kappa V^2)\Big\{\Big[(\kappa-1)V\overline{\mu}+2\kappa V\overline{U}+\frac{\kappa-1}{\kappa}\overline{\nu}$$
$$+2\overline{W}\Big]\kappa\hat{\gamma}-2(1+\kappa)[-1+(1+\kappa)(sx)^2\overline{\rho}](sx)^{-1}\check{\alpha}$$
$$+\frac{1}{2}(1+\kappa)\Big(\frac{1+\kappa}{\kappa}\overline{\nu}-2\overline{W}+(1+\kappa)V\overline{\mu}$$
$$+2\kappa V\overline{U}\Big)sx\mathring{\psi}-(1+\kappa)(\overline{\mu}+V\overline{\nu})\mathring{\eta}+(1+\kappa)(\overline{\mu}$$
$$+V\overline{\nu})(sx)^2\mathring{\chi}\Big\}$$
$$-\left[1+\frac{(1-\kappa)V}{(1-\kappa V^2)sgx}\right]\hat{\omega}+\frac{\kappa(1-V^2)}{(1-\kappa V^2)sgx}\hat{\gamma}, \quad \text{(B21)}$$

$$S(\check{\alpha})=a\sqrt{1-V^2}g\Big\{-\frac{\kappa}{1+\kappa}(sx)^{-1}\hat{\omega}+[\kappa\overline{\mu}+(2\kappa$$
$$-1)\overline{U}]\hat{\alpha}-(sx)^{-1}\mathring{\eta}+\frac{1}{2}(sx)\mathring{\chi}\Big\}-\left(1+\frac{V}{sgx}\right)\check{\alpha}. \quad \text{(B22)}$$

The variable $\check{\alpha}$, which is odd and $O(x)$, is much better behaved than the more obvious definition $\hat{\alpha}\equiv(sx)^{-2}\mathring{\alpha}$. [The combination $\mathring{\eta}+\kappa/(1+\kappa)\hat{\omega}$ is $O(x^2)$ at the center. Numerically, it is easier to divide this by sx in $S(\check{\alpha})$ to obtain an $O(x)$ term than to divide by $(sx)^2$.] The constraints are solved with the matrix M given above and the source terms

$$\check{s}=a^2(-2\overline{\rho}\kappa(sx)\hat{\gamma}+4\overline{\rho}(1+\kappa)\overline{W}(sx)^2\check{\alpha},$$
$$(1-\kappa)\overline{\rho}(sx)^2\hat{\omega}-4(1+\kappa)\overline{\rho U}(sx)^3\check{\alpha},$$
$$2\overline{\rho}\hat{\omega}-8(1+\kappa)\overline{\rho U}(sx)\check{\alpha}). \quad \text{(B23)}$$

The boundary conditions are Eq. (B15) with $(sx)^{-1}\mathring{\omega}$ replaced by $\hat{\omega}$.

APPENDIX C: $l\geq 2$ POLAR PERTURBATION EQUATIONS

In order to work with variables that are regular and $O(1)$ at the origin for any l, we redefine them as $\chi=r^{l+2}\overline{\chi}$, $\psi=r^{l+1}\overline{\psi}$ and $k=r^l\overline{k}$, as in [9]. In order to obtain a first-order formulation, we introduce the frame derivatives of the barred quantities with respect to the fluid frame. From Eqs. (87)–(89) of [9], the equations then take the form

$$(\dot{\overline{\chi}})\dot{}-(\overline{\chi}')'-2(\mu-U)r^{-1}\overline{\psi}'$$
$$=-r^{-(l+2)}S_\chi-2(l+2)U\dot{\overline{\chi}}-(l+2)[(l+2)U^2+\dot{U}]\overline{\chi}$$
$$+2(l+2)W\overline{\chi}'+(l+2)[(l+2)W^2+W']\overline{\chi}$$
$$+2(\mu-U)r^{-1}(l+1)W\overline{\psi}\equiv e^{(l+4)\tau}S_1, \quad \text{(C1)}$$

$$(\overline{\chi}')\dot{}-(\dot{\overline{\chi}})'=\nu\dot{\overline{\chi}}-\mu\overline{\chi}'\equiv e^{(l+4)\tau}S_2, \quad \text{(C2)}$$

$$(\dot{\overline{k}})\dot{}-\kappa(\overline{k}')'+2\kappa Ur\overline{\psi}'$$
$$=-r^{-l}S_k-2lU\dot{\overline{k}}-l(lU^2+\dot{U})\overline{k}+2\kappa lW\overline{k}'$$
$$+\kappa l(lW^2+W')\overline{k}-2\kappa Ur(l+1)W\overline{\psi}\equiv e^{(l+2)\tau}S_3, \quad \text{(C3)}$$

$$(\overline{k}')\dot{}-(\dot{\overline{k}})'=\nu\dot{\overline{k}}-\mu\overline{k}'\equiv e^{(l+2)\tau}S_4, \quad \text{(C4)}$$

$$(\overline{\psi})\dot{}=-r^{-(l+1)}S_\psi-(l+1)U\overline{\psi}\equiv e^{(l+2)\tau}S_5, \quad \text{(C5)}$$

where the source terms S_χ, S_k and S_ψ are given in Eqs. (A1)–(A3) of [9]. The second and fourth equations are just the commutation relations between the dot and prime derivatives. Here they serve as auxiliary evolution equations for $\overline{\chi}'$ and $\overline{k}'$. To these five equations we add the trivial evolution equations $(\overline{\chi})\dot{}=\dot{\overline{\chi}}$ and $(\overline{k})\dot{}=\dot{\overline{k}}$.

For our particular application to a self-similar background we further rescale these first-order variables to obtain the final dynamical variables

$$\mathring{\chi}=e^{-(l+2)\tau}\overline{\chi}, \quad \tilde{\chi}=e^{-(l+3)\tau}(\overline{\chi})\dot{}, \quad \hat{\chi}=e^{-(l+3)\tau}(\overline{\chi})', \quad \text{(C6)}$$

$$\mathring{k}=e^{-l\tau}\overline{k}, \quad \tilde{k}=e^{-(l+1)\tau}(\overline{k})\dot{}, \quad \hat{k}=e^{-(l+1)\tau}(\overline{k})',$$
$$\mathring{\psi}=e^{-(l+1)\tau}\overline{\psi}. \quad \text{(C7)}$$

The variables with a circle or a tilde are even and $O(1)$ at the center, while the variables with a hat are odd and $O(x)$. The perturbed spacetime remains CSS if and only if all seven perturbation variables are independent of τ. These seven variables obey evolution equations without any constraints, except for the trivial ones that arise when one writes a wave equation in first-order form, given below in Eqs. (C15), (C16). Applying the same rescaling to the source terms S_1 to S_5, we obtain, in the notation $Bu\equiv S(u)$, the source terms in the evolution equations for $\tilde{\chi}$ to $\mathring{\psi}$. To these we add two evolution equations $\mathring{\chi}$ and $\mathring{k}$, which have only source terms, but no x derivatives. We obtain them by solving Eqs. (A1), (A2) for $f_{,\tau}$ in terms of $\dot{f}$ and f'. Putting all seven source terms together, we have

$$S(\tilde{\chi})=\frac{a\sqrt{1-V^2}}{g}\frac{S_1+VS_2+2V(\bar{\mu}-\bar{U})(sx)^{-1}S_5}{1-V^2}-(l+3)\tilde{\chi}, \tag{C8}$$

$$S(\hat{\chi})=\frac{a\sqrt{1-V^2}}{g}\frac{VS_1+S_2+2V^2(\bar{\mu}-\bar{U})(sx)^{-1}S_5}{1-V^2}-(l+3)\hat{\chi}, \tag{C9}$$

$$S(\tilde{k})=\frac{a\sqrt{1-V^2}}{g}\frac{S_3+\kappa VS_4-2V\kappa\bar{U}sxS_5}{1-\kappa V^2}-(l+1)\tilde{k} \tag{C10}$$

$$S(\hat{k})=\frac{a\sqrt{1-V^2}}{g}\frac{VS_3+S_4-2V^2\kappa\bar{U}sxS_5}{1-\kappa V^2}-(l+1)\hat{k}, \tag{C11}$$

$$S(\mathring{\psi})=\frac{a\sqrt{1-V^2}}{g}S_5-(l+1)\mathring{\psi}, \tag{C12}$$

$$S(\mathring{\chi})=\frac{as}{\sqrt{1-V^2}}\left[\left(Vx+\frac{1}{sg}\right)\tilde{\chi}-\left(x+\frac{V}{sg}\right)\hat{\chi}\right]-(l+2)\mathring{\chi}, \tag{C13}$$

$$S(\mathring{k})=\frac{as}{\sqrt{1-V^2}}\left[\left(Vx+\frac{1}{sg}\right)\tilde{k}-\left(x+\frac{V}{sg}\right)\hat{k}\right]-l\mathring{k}. \tag{C14}$$

Finally, solving Eqs. (A1),(A2) for $f_{,x}$ in terms of $\dot{f}$ and f', we obtain two constraint equations, that is, equations that do not contain τ derivatives. They are

$$\mathring{\chi}_{,x}=\frac{as}{\sqrt{1-V^2}}(\hat{\chi}-V\tilde{\chi}), \tag{C15}$$

$$\mathring{k}_{,x}=\frac{as}{\sqrt{1-V^2}}(\hat{k}-V\tilde{k}). \tag{C16}$$

The intermediate source terms S_i are

$$S_1=-[3\bar{\mu}+2(l+2)\bar{U}]\tilde{\chi}+[5\bar{\nu}+2(l+1)\bar{W}]\hat{\chi}+4(\bar{U}-\bar{\mu})(sx)^{-2}\tilde{k}+2[(l-1)(\bar{\mu}-\bar{U})\bar{W}+2\overline{\mu\nu}+e^{-2\tau}(\mu'-\dot{\nu})](sx)^{-1}\mathring{\psi}$$
$$+\left[-2l\bar{U}^2+(4l+8)\overline{\nu W}-(2l+8)\overline{\mu U}-(2l^2+4)(sx)^{-2}\frac{m}{r}+[-(1-\kappa)l+2\kappa+2]\bar{\rho}+4\bar{\nu}^2\right]\mathring{\chi}$$
$$+4\left[\bar{\nu}^2+\left(\bar{\rho}-3(sx)^{-2}\frac{m}{r}\right)+(l+1)(\bar{U}-\bar{\mu})\bar{U}\right](sx)^{-2}\mathring{k}, \tag{C17}$$

$$S_2=\bar{\nu}\tilde{\chi}-\bar{\mu}\hat{\chi}, \tag{C18}$$

$$S_3=-(1+\kappa)\bar{U}(sx)^2\tilde{\chi}+(1-\kappa)\bar{W}(sx)^2\hat{\chi}-[(4+2\kappa+2l)\bar{U}+\kappa\bar{\mu}]\tilde{k}+[\bar{\nu}+2\kappa(l+1)\bar{W}]\hat{k}+2[(1-\kappa)\overline{\mu W}-(1+\kappa)\overline{\nu U}$$
$$-(\kappa l+2\kappa+1)\overline{UW}](sx)\mathring{\psi}+\left\{-[(1+\kappa)l+2+4\kappa](sx)^2\bar{U}^2+[(1-\kappa)l-2\kappa](sx)^2\bar{W}^2+\frac{1-\kappa}{2}(l^2+l+2)\right.$$
$$\left.-4\kappa(sx)^2\overline{\mu U}+4\kappa(sx)^2\bar{\rho}\right\}\mathring{\chi}+\left\{[-(1-\kappa)l^2-(\kappa+3)l-2-2\kappa]\bar{U}^2-[2\kappa l^2-(1-\kappa)l-4](sx)^{-2}\frac{m}{r}\right.$$
$$\left.-4\kappa\overline{\mu U}+4\kappa\bar{\rho}\right\}\mathring{k}, \tag{C19}$$

$$S_4=\bar{\nu}\tilde{k}-\bar{\mu}\hat{k}, \tag{C20}$$

$$S_5=-(sx)\hat{\chi}-[(l+1)\bar{U}+2\bar{\mu}]\mathring{\psi}-[(l+2)\bar{W}+2\bar{\nu}](sx)\mathring{\chi}-2\bar{\nu}(sx)^{-1}\mathring{k}. \tag{C21}$$

We have used the background equations of motion, and have introduced the new coefficient $e^{-2\tau}(\mu'-\dot{\nu})$, which is again independent of τ on a CSS background. Note that all coefficients in the evolution equations are explicitly regular when one takes into account that $\overline{U}-\overline{\mu}=O(x^2)$, $\overline{\rho}-(m/r)/(sx)^2=O(x^2)$ and $e^{-2\tau}(\mu'-\dot{\nu})=O(x)$. The two terms $2(l+1)\overline{W}\hat{\chi}$ and $2\kappa(l+1)\overline{W}\hat{k}$ are the equivalent of the term $2(l+1)\phi'/r$ of the toy model wave equation that we discussed above. They can be regularized in the same way.

APPENDIX D: A TOY MODEL FOR THE EVOLUTION EQUATIONS

We have tested various numerical methods on a toy model, the scalar wave equation in flat spacetime. This model is also useful as an illustration of the types of variable and the methods we use.

Let Φ obey the free wave equation on the flat spacetime $ds^2=-dt^2+dr^2+r^2d\Omega^2$. We make the ansatz

$$\Phi=\sum_{l,m}\phi_{lm}(r,t)Y_{lm}(\theta,\varphi). \tag{D1}$$

We now consider a particular value of l and m, and drop these suffixes. Then ϕ_{lm} obeys

$$-\phi_{,tt}+\phi_{,rr}+\frac{2}{r}\phi_{,r}-\frac{l(l+1)}{r^2}\phi=0. \tag{D2}$$

As in [9] we introduce the rescaled and first-order variables

$$\overline{\phi}\equiv r^{-l}\phi, \quad \overleftarrow{\phi}\equiv\overline{\phi}_{,t}, \quad \overline{\phi}'\equiv\overline{\phi}_{,r}. \tag{D3}$$

$\Phi(t,r,\theta,\varphi)=\Phi(t,x,y,z)$ is analytic in Cartesian coordinates at the origin if and only if ϕ is analytic in r with only even powers of r. In this sense $\overline{\phi}$ and $\overleftarrow{\phi}$ are even functions of r, and are generically finite and nonzero at $r=0$, and $\overline{\phi}'$ is odd and generically $O(r)$ at $r=0$.

We now go over to self-similarity coordinates x and τ defined in Eq. (4) (with $s=1$). In order to mimic the fluid perturbation equations, we rescale the first-order variables once again as

$$\mathring{\phi}\equiv e^{-n\tau}\overline{\phi}, \quad \tilde{\phi}\equiv e^{-(n+1)\tau}\overleftarrow{\phi}, \quad \hat{\phi}\equiv e^{-(n+1)\tau}\overline{\phi}'. \tag{D4}$$

The most natural choice of n for the toy model is $n=0$, but for the fluid perturbations, it will be fixed by the requirement that the perturbed spacetime remains self-similar if the perturbation variables do not grow or decay with τ. We therefore leave it free. We finally obtain the first-order system

$$\tilde{\phi}_{,\tau}=-x\tilde{\phi}_{,x}+\hat{\phi}_{,x}+2(l+1)\frac{\hat{\phi}}{x}-(n+1)\tilde{\phi}, \tag{D5}$$

$$\hat{\phi}_{,\tau}=\tilde{\phi}_{,x}-x\hat{\phi}_{,x}-(n+1)\hat{\phi}, \tag{D6}$$

$$\mathring{\phi}_{,\tau}=\tilde{\phi}-x\hat{\phi}-n\mathring{\phi}. \tag{D7}$$

There is also the trivial constraint

$$\mathring{\phi}_{,x}=\hat{\phi} \tag{D8}$$

that follows from the definition of the first-order variable $\hat{\phi}$.

One significant property that the toy model has in common with the full perturbation equations is that $\mathring{\phi}$ and $\tilde{\phi}$ are even and generically nonzero at $x=0$ while $\hat{\phi}$ is odd and generically $O(x)$. All terms except $\hat{\phi}/x$ are explicitly regular, and do not require special treatment at the origin. In particular, there is no term of the type ϕ/x^2 left. Experience shows that terms of the form $\hat{\phi}/x$, where $\hat{\phi}$ is an odd function of x and $O(x)$, can be regularized without giving rise to instabilities, while division by x^2 is much more troublesome.

In other, unimportant, aspects the toy model is simpler than the full perturbation equations. As there is no fluid frame in this toy model, we choose the dot and prime to be frame derivatives with respect to the constant r frame. As the spacetime is flat, the dot and prime derivatives commute. Finally, in the toy model $\mathring{\phi}$ does not couple back to $\hat{\phi}$ and $\tilde{\phi}$, and therefore plays only a passive role.

APPENDIX E: FINITE DIFFERENCING

For the evolution equations (24) at hand, the eigenvalues and eigenvectors of the matrix A can be calculated in closed form. The eigenvalues of A are $dx/d\tau$ on characteristics of the equations: fluid world lines, radial light rays, and radial matter (sound wave) characteristics. The characteristics are symmetric around the line $x=0$, but with increasing x they tip over until at sufficiently large x all eigenvalues are negative. This means that at large x information travels only from smaller to larger x. The reason for this is of course that while $x=0$ and lines of small constant x are timelike, lines of large constant x are spacelike. The ''outer boundary'' $x=x_{\max}$ of our numerical domain $0\leqslant x\leqslant x_{\max}$ is therefore a future spacelike boundary, and so no boundary condition is required there.

In order to use it to obtain a free boundary condition, we make the numerical method reflect the propagation of information, so that at $x=x_{\max}$ all x derivatives are calculated using one-sided finite differences. Following [14], we split A into a left and a right-moving part. Let V be the matrix of (column) eigenvectors of A. Let Λ be the diagonal matrix composed of the corresponding eigenvalues. Then $A=V\Lambda V^{-1}$. Let Λ_+ be Λ with zeros in the place of the negative eigenvalues, and let Λ_- be Λ with zeros in the place of the positive eigenvalues. Then define $A_\pm=V\Lambda_\pm V^{-1}$. It is clear that $A=A_++A_-$. We now use A_+ with left derivatives and A_- with right derivatives

$$\frac{du_j^n}{d\tau}=(A_+D_+u_j^n+A_-D_-u_j^n+Bu_j^n), \tag{E1}$$

with the one-sided derivatives

$$D_+u_j^n=\frac{u_{j+1}^n-u_j^n}{\Delta x}, \quad D_-u_j^n=\frac{u_j^n-u_{j-1}^n}{\Delta x}. \tag{E2}$$

Here the coefficient matrices $A_\pm$, B and C are evaluated at x_j. After each time step, the constrained variables w are obtained at τ^{n+1} from the u^{n+1}. This scheme is first-order accurate in x. (Note that we have not discretized in τ yet.) Left differences at $x=0$ are evaluated using ghost points based on the fact that all grid functions u are either even or odd in x. This scheme can be thought of as the Godunov method applied to a linear equation, and we shall refer to it as the first-order Godunov scheme, or GD1. To obtain a second independent finite differencing scheme, we have also used the second-order one-sided derivatives

$$D_+u^n_j=\frac{4u^n_{j+1}-3u^n_j-u^n_{j+2}}{2\Delta x},$$

$$D_-u^n_j=-\frac{4u^n_{j-1}-3u^n_j-u^n_{j-2}}{2\Delta x}. \tag{E3}$$

We shall refer to this scheme as GD2. At the outer boundary $x=x_{\max}$, no right derivatives are required, as there all information travels from the left to the right. (A_+ vanishes.) All variables u are either even or odd functions of x. At the inner boundary $x=0$, left derivatives are calculated using fictitious grid points at negative x that are obtained as $u(-x)=\pm u(x)$. By construction, the Godunov method has the advantage that it does not require a special outer boundary conditions. Unexpectedly, it also has the advantage that it handles terms of the form $\hat\phi/x$ term at the center without any special treatment. It is also completely free from high-frequency grid modes. This last property is less surprising when one thinks of GD1 as centered differencing plus a dissipative term [14].

We have also implemented a more standard finite differencing scheme based on centered differences in x, with a (first or second order) one-sided derivative at the outer boundary $x=x_{\max}$. The center is again handled by ghost points, using $u(-x)=\pm u(x)$. Using naive centered differences, the code is unstable at the center because of the source term $2(l+1)\hat\phi/x$ in the toy model, and similar terms in the perturbation equations. A well-known remedy is to include this source term into the transport terms in the way suggested by the identity

$$\hat\phi_{,x}+\frac{2(l+1)}{x}\hat\phi=(2l+3)\frac{\partial(x^{2l+2}\hat\phi)}{\partial(x^{2l+3})}. \tag{E4}$$

In the toy model wave equation this procedure slows down the central instability enough so that it can be suppressed by numerical viscosity. We have added a centered difference expression for $u_{,\tau}=cu_{,xx}+\cdots$, with c of the order of 10^{-3}. However, numerical viscosity falsifies the results too much both in the toy model and in the actual problem, and has therefore not been used in any of the results of this paper. We shall refer to centered differencing with Eq. (E4) as CD3, and without as CD4.

APPENDIX F: WEAK SOLUTIONS

We now discuss a problem that affects the fluid and metric perturbations that we want to investigate, but that is already present and more easily understood in the toy model.

The spacetime point $r=t=0$ is singled out in the self-similarity coordinates x and τ, but it is not preferred on the flat background. A solution arising from generic C^2 initial data at $t=t_0<0$ has finite t and r derivatives at $t=r=0$. The coordinates x and τ, however, have been designed to ''zoom in'' on this spacetime point: we are looking at a smooth solution on ever smaller scales. Therefore, as $\tau\to\infty$, a generic solution of the toy model wave equation should behave at large τ as

$$\mathring\phi\to\overline{\phi}(0,0)e^{-n\tau},\quad \tilde\phi\to\overline{\phi}_{,t}(0,0)e^{-(n+1)\tau},$$

$$\hat\phi\to\frac{1}{2}\overline{\phi}_{,rr}(0,0)e^{-(n+2)\tau}. \tag{F1}$$

In deriving this fall-off we have assumed that ϕ is at least twice differentiable everywhere. But as $x=1$ is a characteristic of the wave equation, ϕ and its derivatives are allowed to be discontinuous there. In particular, data on $x>1$ do not influence the solution on $x\leqslant 1$. Therefore, solutions exist that vanish on $x\leqslant 1$ for all τ but not for $x>1$. In particular, making a power-series ansatz for the region $x>1$,

$$\tilde\phi(x,\tau)=e^{\lambda\tau}[\,\tilde\phi_1(x-1)+\tilde\phi_2(x-1)^2+\cdots],$$

$$\hat\phi(x,\tau)=e^{\lambda\tau}[\,\hat\phi_1(x-1)+\hat\phi_2(x-1)^2+\cdots], \tag{F2}$$

we find a formal solution with $\lambda=l-1-n$, which is slower than the expected falloff by l. We believe that a corresponding weak solution of the wave equation exists that is analytic for $x>1$ (and vanishes for $x\leqslant 1$), but have not proved it. A finite difference counterpart certainly does exist, and for GD1 and GD2 it falls off (or grows, depending on n and l) with the calculated value of λ. It therefore dominates over the generic smooth solution at large τ. We want to exclude it in studies of critical collapse, as we are interested only in the time evolution of smooth perturbation initial data. Numerical schemes, however, do not distinguish between smooth and unsmooth data, and this solution turns up in some of them, hiding the everywhere C^2 solutions we are interested in. In the future we shall refer to these as ''weak solutions at the light cone'' or simply ''weak modes,'' We should stress that, depending on the finite differencing scheme, weak solutions of the finite difference equations may or may not converge to weak solutions of the continuum equations, but they are always there.

We find that both Godunov schemes when applied to the toy model wave equations develop weak solutions that are continuous but not differentiable at $x=1$. For GD1, the finite difference mode corresponding to the weak solution can be analyzed easily. $u_{,\tau}$ at the first grid point with $x>1$ depends only on u at that point, and on the next point to the left—but

there all fields vanish in a weak solution. A calculation shows that u at the first grid point with $x>1$ depends exponentially on τ. The exponent is either $\lambda=l-1-n+O(\Delta x)$, which is the continuum weak solution, or $\lambda=-2/\Delta x+O(1)$, which is a finite differencing artifact that decays quickly.

In GD1, the dominant weak solution is clearly not differentiable at $x=1$, and this also shows up in independent residual evaluation as a sharp peak. If the last grid point is exactly $x=1$, the numerical domain can consistently be truncated there, and no weak modes can arise. Because of its wider stencil GD2 is not completely causal, and so part of the weak mode propagates to $x<1$. The numerical equivalent of the weak mode therefore appears differentiable at $x=1$, but there is still a peak there in independent residual evaluation, although less sharp. If we attempt to truncate GD2 at $x=1$, we need to introduce an explicit boundary condition there. Doing this by using a first-order right derivative, or a centered derivative at $x=1-\Delta x$ introduces spurious reflections at the boundary. Without truncation, we have tried updating the grid point $x=1+\Delta x$ by interpolation from the neighboring grid points. This does not suppress the weak mode. Updating the three points $x=1$, $x=1+\Delta x$ and $x=1+2\Delta x$ by interpolation results in a different spurious mode. This holds both for GD1 and GD2.

APPENDIX G: IMPOSING THE CONSTRAINTS

Some perturbation equations contain only x derivatives, and so are constraints rather than evolution equations. Even the free wave equation has such a constraint when it is written in first-order form. Constraints of the form (D8) are solved by integration from the center out, using the trapezoid rule,

$$\mathring{\phi}^{i+1}=\mathring{\phi}^{i}+\frac{\Delta x}{2}(\hat{\phi}^{i+1}+\hat{\phi}^{i}), \tag{G1}$$

where the starting point $\mathring{\phi}$ at the center is determined by the evolution equation. This method is second-order accurate. We also use the exact of these finite difference equations to obtain $\hat{\phi}$ from $\mathring{\phi}$ by differentiation.

Time evolution commutes with the constraints in the continuum limit, but in the discretized equations this is only approximately true. In order to find the modes, we need a matrix T that acts only on a set of functions u that can be freely specified in the initial data and is therefore of full rank. We start with a larger matrix T' and have to reduce it using a numerical solution of the constraints. This reduction, however, is not unique, and although different reductions are equivalent in the continuum equations, they are not in the finite difference equations.

We discuss these issues in the toy model. The matrix T' acts on $\mathring{\phi}$, $\hat{\phi}$ and $\tilde{\phi}$, so that T' is a $(3N)^2$ matrix. There are two natural choices for the free variables on which T acts: either $\mathring{\phi}$ and $\tilde{\phi}$, or the functions $\hat{\phi}$ and $\tilde{\phi}$ plus the number $\mathring{\phi}(0)$. Note that $\hat{\phi}(0)=0$ by definition, so that in either case T is a $(2N)^2$ matrix.

We denote the constraint solution scheme (G1) by I (for integration) and its numerical inverse by D (for differentiation). In loose matrix notation we can then write the first possibility as

$$u=\begin{pmatrix}\tilde{\phi}\\ \mathring{\phi}\end{pmatrix},\quad T_1\equiv\begin{pmatrix}1&0&0\\0&0&1\end{pmatrix}T'\begin{pmatrix}1&0\\0&D\\0&1\end{pmatrix}, \tag{G2}$$

and

$$u=\begin{pmatrix}\tilde{\phi}\\ \hat{\phi}\end{pmatrix},\quad T_2\equiv\begin{pmatrix}1&0&0\\0&1&0\end{pmatrix}T'\begin{pmatrix}1&0\\0&1\\0&I\end{pmatrix}. \tag{G3}$$

We find that T_2 works much better than T_1, in having grid modes. This is not surprising given that integration has a smoothing property. An alternative to T_1 is to re-impose the constraints by integration after evolution,

$$u=\begin{pmatrix}\tilde{\phi}\\ \mathring{\phi}\end{pmatrix},\quad T_3\equiv\begin{pmatrix}1&0&0\\0&I&0\end{pmatrix}T'\begin{pmatrix}1&0\\0&D\\0&0\end{pmatrix}. \tag{G4}$$

But the matrix T_3 is similar to the matrix T_2,

$$T_2=\begin{pmatrix}1&0\\0&D\end{pmatrix}T_3\begin{pmatrix}1&0\\0&I\end{pmatrix}, \tag{G5}$$

and so T_2 and T_3 have the same eigenvalues, although of course not the same eigenvectors. This is borne out numerically up to small rounding errors.

In the spherical and the $l=1$ polar perturbations, nontrivial constraint equations arise which are of the form

$$xu_{,x}=M(x)u+s, \tag{G6}$$

where u stands for a subset of variables, and the source terms s are linear in the other variables, already known at this time level. The coefficient matrix $M(x)$, an even function of x, is typically nonzero at the origin. The ODE is therefore singular at $x=0$. We look for solutions $u(x)$ that are even regular functions of x. These obey $M(0)u(0)=s(0)$. From this boundary condition, the ODEs are solved by the implicit, second-order accurate scheme

$$y_{i+1}=(1-\epsilon M_{i+1})^{-1}[(1+\epsilon M_i)y_i+\epsilon(s_i+s_{i+1})],$$

$$\epsilon\equiv(x_{i+1}-x_i)/(x_{i+1}+x_i). \tag{G7}$$

[1] M.W. Choptuik, Phys. Rev. Lett. **70**, 9 (1993).
[2] C. Gundlach, Living Reviews 1999-4, published electronically as http://www.livingreviews.org. See also Phys. Rep. (in preparation).
[3] T. Koike, T. Hara, and S. Adachi, Phys. Rev. Lett. **74**, 5170 (1995).
[4] C.R. Evans and J.S. Coleman, Phys. Rev. Lett. **72**, 1782 (1994).
[5] D. Maison, Phys. Lett. B **366**, 82 (1996).
[6] T. Koike, T. Hara, and S. Adachi, Phys. Rev. D **59**, 104008 (1999).
[7] D.W. Neilsen and M.W. Choptuik, Class. Quantum Grav. **17**, 761 (2000).
[8] C. Gundlach, Phys. Rev. D **57**, R7075 (1998).
[9] C. Gundlach and J.M. Martín-García, Phys. Rev. D **61**, 084024 (2000).
[10] J.M. Martín-García and C. Gundlach, Phys. Rev. D **59**, 064031 (1999).
[11] C. Gundlach, Phys. Rev. D **57**, R7080 (1998).
[12] C. Gundlach, Phys. Rev. D **55**, 695 (1997).
[13] C. Gundlach, Phys. Rev. D **65**, 064019 (2002).
[14] R.J. LeVeque, *Numerical Methods for Conservation Laws* (Birkhäuser, Basel, 1992).